Work Package 4: Which interactions exist between stratospheric ozone depletion and the greenhouse effect?

Contribution of DLR

Overview

The research activities of DLR covered the following fields:

- Definition, realisation and analysis of a transient long-term model simulation (1960 – 1999) employing the coupled chemistry-climate model (CCM) ECHAM4.L39(DLR)/CHEM;
- first investigation of impacts of stratospheric aerosol changes produced by volcanic eruptions on dynamical and chemical processes in the lower stratosphere (jointly with MPI-MIPS);
- time-dependent study of the ozone evolution driven by both chemical and dynamical changes of the lower stratosphere, i.e., comparison with observations (jointly with DWD, MPI-MAECHAM, MPI-C);
- further development of E39/C, i.e., implementation of parameterisation of large solar zenith angles (SZAs) and related sensitivity experiments with E39/C (jointly with MPI-C).

Transient model simulation with E39/C

In this study, the interactively coupled CCM ECHAM4.L39(DLR)/CHEM (hereafter: E39/C) is used for a transient model simulation covering the time period from 1960 to 1999. The model system has previously been applied for several investigations, but there exclusively results of time-slice experiments were used. Detailed information about E39/C is given in Hein et al. (2001). In the current model version, the rate coefficients have been updated using JPL (2000). In addition, two heterogeneous reactions on stratospheric aerosol have been included ($ClONO_2 + HCl \rightarrow Cl_2 + HNO_3$ and $HOCl + HCl \rightarrow Cl_2 + H_2O$). The transport of chlorine components has been improved by transporting both, the total chlorine and the partitioning of chlorine species, to minimise numerical diffusion in regions with lower vertical resolution.

The horizontal resolution of the model is T30, i.e., dynamic processes have an isotropic resolution of about 670 km. The corresponding Gaussian transform latitude-longitude grid, on which the model physics, chemistry, and tracer transport are calculated, has a mash size of 3.75° x 3.75°. In the vertical, E39/C has 39 layers from the surface to 10 hPa (Land et al., 2002). CHEM (Steil et al., 1998) is based on the family concept. It describes relevant stratospheric and tropospheric O_3 related homogeneous chemical reactions and heterogeneous chemistry on PSCs and sulfate aerosols, it does not consider bromine chemistry. E39/C includes online feedbacks of dynamics, chemistry, and radiative processes: Chemical tracers are advected by the simulated winds. The net heating rates and photolysis rates, in turn, are calculated using the actual 3D distributions of the radiatively active gases O_3, CH_4, N_2O, H_2O and CFCs, and the 3D cloud distribution. The model climatology has been extensively validated; specifically, analyses on the model's performance in the Arctic stratosphere have been carried out (e.g., Hein et al., 2001; Schnadt et al., 2002; Austin et al., 2003).

Design of the transient simulation

The transient integration of E39/C, which covers the period from 1960 to 1999, is preceded by a spin-up period of 10 years. The simulation aims to reproduce the climatic evolution over recent 40 years including natural as well as anthropogenic forcings. The natural factors considered in the transient integration are the 11-year solar cycle, the QBO, and the chemical and direct radiative effects of the major volcanic eruptions of Agung in 1963, El Chichon in 1982, and Pinatubo in 1991. The anthropogenic influence is represented by specifying atmospheric concentrations of the most important WMGHGs, chlorofluorocarbons (CFCs), and nitrogen oxide emissions.

The sea surface temperatures (SSTs) are prescribed as monthly means following the global sea ice and sea surface temperature (HadISST1) data set from the UK Met Office Hadley Centre. This data set is based on blended satellite and in situ observations. Gaps in the sea ice coverage caused by interpolation to the model grid have been removed by a careful consistency check.

The effects of large volcanic eruptions are considered in the transient simulation. In the chemistry module, sulfate aerosol surface area densities are partly derived from observations as follows: The original data set which is used consists of monthly and zonally averaged sulfate aerosol surface area density (WMO, 2003). It was deduced from satellite-based extinction measurements (SAGE I, SAGE II, SAM II, and SME). This data set (1979-1995) does not fully cover the simulation period 1960-1999. Most importantly, the Agung eruption in 1963 was not included. As a remedy, the well-documented years (1982-1985) following the eruption of El Chichon has been adapted and associated with the period 1963-1966 with modifications to account for differences in total mass of sulfate aerosols inside the stratosphere, in maximum height of the eruption plumes, and in the volcanos' geographical location. Above the maximum vertical extent of Agung's eruption plume the annual mean of 1979 has been incorporated. In 1979 the total mass of stratospheric sulfate aerosol was possibly close to it's background value, being maintained by a permanent supply of tropospheric sulfur species. For the time periods 1960-1962 and 1968-1978 the annual mean of 1979 has been adopted, for the period 1996-1999 the annual mean of 1995. Additionally, the data set has been interpolated linearly both from 177 to 16 vertical levels, and from 18 latitudes to 48 latitudes.

Eruption-related radiative heating is implemented in E39/C using pre-calculated monthly and zonally mean net heating rates. These rates have been modelled previously in an ECHAM4(T42)/L19 (L19 = 19 vertical layer) Pinatubo experiment, with a forcing by realistic aerosol spatial-time distributions (Kirchner et al., 1999). The original data set extends from July 1991 to April 1993. Thus, only part of eruption-influenced time span was available, e.g., June 1991 (month of eruption) is missed. Therefore, for June 1991 the radiative forcing has been taken as “0.5 x July 1991 values” and an exponential decay has been adopted in the period from May 1993 to July 1993. With regard to the Agung and El Chichon eruptions, there the Pinatubo net heating rates have also been used without major changes, because there were strong hints for a similar radiative heating. Finally, the data have been interpolated from L19 to L39 (i.e. number of vertical layer within E39/C).

The QBO is generally described by zonal wind profiles measured at the equator. Radio-sonde data from Canton Island (1953-1967), Gan/Maledives (1967-1975) and Singapore (1976-2000) have been used to develop a time series of measured monthly mean winds at the equator. This data set covers the lower stratosphere up to 10 hPa. It is used to assimilate the QBO in E39/C, such that the QBO is synchronised with other external inter-annual variations prescribed in this experiment. Here, the QBO is assimilated by a linear relaxation method, also known as "nudging". This assimilation is applied equatorward of 20° latitude from 90 hPa up to the highest layer of the model centred at 10 hPa. The relaxation time scale has been set to 7 days within the QBO core domain. Outside of this core domain the time scale depends on latitude and pressure. The assimilated QBO compares well with the observed phase state and the observed amplitudes of the westerlies and easterlies).

The influence of the solar cycle is parameterised according to the intensity of the 10.7 cm radiation of the sun (data available since 1947 at: http://www.drao-orf.hia-iha.nrc-cnrc.gc.ca/icarus/www/sol_home.shtml). Radiation is considered in two spectral intervals, whereas photolysis rates are calculated in 8 spectral intervals (Landgraf and Crutzen, 1998). Solar intensity is used for the calculation of radiation in the model. The two short-wave intervals are used in the radiation scheme considering continuum scattering, grey absorption, water vapour and uniformly mixed gases transmission functions and ozone transmission.

Continuously changing mixing ratios of the most relevant well-mixed greenhouse gases (CO_2, N_2O, CH_4) and carbon monoxide (CO) are prescribed at the Earth's surface according to IPCC (2001).

Nitrogen oxide emissions at the Earth's surface (both, natural and anthropogenic), from lightning, and from aircraft are considered. The horizontal distribution of NO_x from industry is based on Bekovitz et al. (1996) and its temporal development has been adapted to match the IPCC (2001) values. Emission rates from 1960 to 1999 are assumed to be almost constant around 1.6%/year (IPCC, 1999).

The industry emissions include surface transport, which has been separated according to Matthes (2003), which contributes by approximately 30\% to the total industry NO_x emissions. Ship emissions are subtracted from the global dataset (Benkovitz et al., 1996). Instead, a ship emission inventory with 1993 annual global NO_x emissions of 3.08 Tg(N) is used. Trend estimates for the time period 1970 to 2000 have been adopted from Koehler (2003). Using information on the development of the global ship fleet, these values have been further scaled down to estimate total NO_x emissions for the time period 1960 to 1970.

Nitrogen oxide emissions from biomass burning are based on Hao et al. (1990) and are revised using ASTR fire counts (David Lee, pers. comm., and TRADEOFF-report, 2002). The trend rates are roughly 0.3%/year (IPCC, 1999). The global NO_x soil emissions by micro-biological production are assumed not to change over the four. Aircraft NO_x emissions are based on a data set for 1990 (Schmitt and Brunner, 1997). Previous to 1990 trends are extrapolated using IPCC (1999). For the period 1990 to 1999 an exponential interpolation has been applied. Lightning NO_x emissions are calculated interactively, based on the predicted mean mass flux in the updraft of deep convective clouds (see previous section), resulting in a mean annual emission of 5.16 Tg(N).

To take into account exchange processes from the upper stratosphere upper boundary conditions are adopted for the two families ClX and NO_y at 10 hPa. They are largely responsible for the lower stratospheric nitrogen oxides and chlorine concentrations. Monthly mean concentrations are taken from results of the 2D middle atmosphere model of Brühl and Crutzen (1993), which has also considered effects of the solar cycle. Since CFCs are not explicitly transported by the model E39/C, they are included based on results from the 2D model (depending on latitude and altitude), and serve as a source for Cl_y by photolysis, within the model domain.

The development of CFC concentrations is in agreement with recent assumptions (WMO, 2003). Stratospheric total chlorine (= Cl_y) has been calculated as sum of the simulated ClO_x, $ClONO_2$, HCl fields, and chlorine from the prescribed CFC fields. Its temporal evolution reflects the observed development (WMO, 2003, their figure 1-7).

In the following, we will report on investigations with model results concerning long-term variability and trends. Further investigations are under development and will be published shortly (publication in preparation).

Long-term variability (trends) in E39/C

Total ozone (analysis jointly with MPI-MAECHAM and MPI-C)

In this paragraph global changes of total ozone are presented. Figure WP4-1a shows the development of total ozone for the whole simulation period. It indicates the well known features, e.g., highest ozone values in northern spring time which is highly variable from year-to-year, low ozone values in the tropics with a small seasonal cycle and little inter-annual variability, a relative ozone maximum in mid-latitudes of the Southern Hemisphere in late winter/early spring, and a minimum ozone column above the south polar region. Obviously, the ozone hole (i.e., ozone column values less than 220 Dobson Units) appears for the first time in the year 1982, which is in agreement with observations (Chubachi, 1985; Farman et al., 1985). Another interesting feature which is apparent is that in the Northern Hemisphere in the late 1980s and the first half of the 1990s no high total ozone values (greater 475 DU) are found which indicates a period of at least six years without distinct mid-winter warmings of the stratosphere. There is no other comparable episode in the 40-year simulation. Similar observations where made in the real atmosphere, where between northern winters 1989/90 and

1996/97 no major stratospheric warming occurred which results in obvious ozone losses during these years. Before looking more closely to the trends calculated by the model, it is necessary to evaluate the absolute accuracy of simulated total ozone in E39/C.

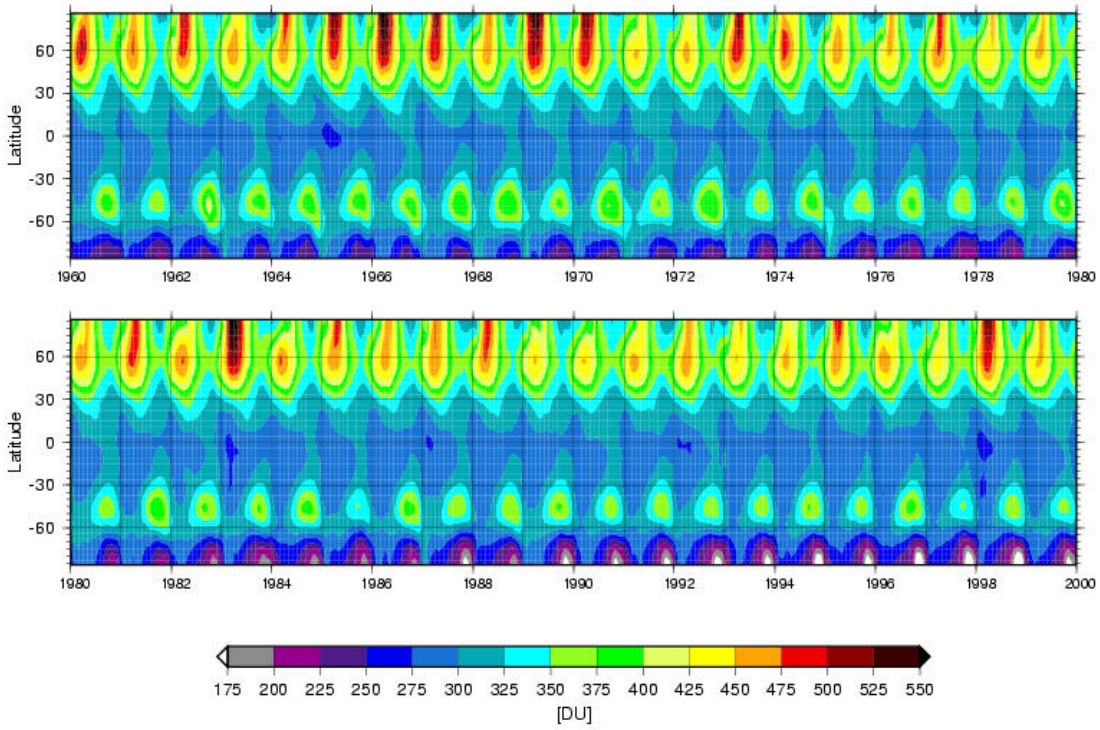

Figure WP4-1a: Development of total ozone (in Dobson Units) derived from the transient simulation obtained with E39/C.

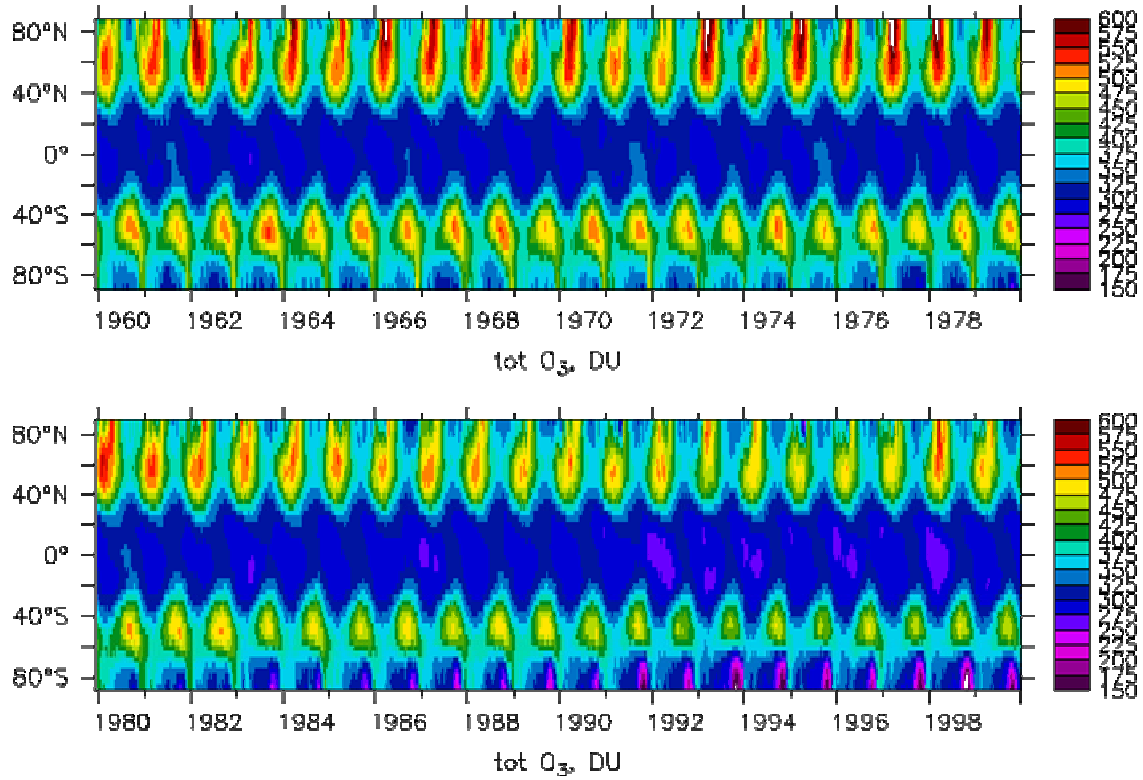

Figure WP4-1b: As Figure WP4-1a, but for results derived from the transient simulation obtained with MAECHAM4/CHEM, carried out with the same boundary conditions as for E39/C.

To allow a direct comparison of results obtained by the E39/C and MAECHAM4/CHEM transient simulations, Figure WP4-1b displays the development of total ozone calculated by MAECHAM4/CHEM. It indicates approximately the same temporal and spatial behaviour as E39/C. There seems to be a somewhat larger inter-annual variability in the Arctic with large depletions in spring 1995 and 1996. Note the very similar behaviour of the 2 models in the late nineties or a period in the early seventies. The Antarctic ozone hole can be as deep as 125DU in the late 1990s. Especially at southern mid-latitudes MAECHAM4/CHEM has a high bias as discussed in Steil et al. (2003). In the tropics total ozone is modulated by QBO (see also WP3).

Figure WP4-2 shows mean climatological total ozone values derived from the E39/C simulation, i.e., the 1960s and 1970s (Fig. WP4-2a), the 1980s and 1990s (Fig. WP4-2b), and measurements from the TOMS instrument for the years 1985 to 1997 (Fig. WP4-2c). A comparison of Figs. WP4-2b and WP4-2c indicates that E39/C is able to reproduce the main features (e.g., regional distribution, seasonal cycle) in qualitative agreement with TOMS observations. In the Northern Hemisphere and the tropics, the model calculates total ozone values which are about 10 to 15% higher than those values derived from TOMS. These model results confirm the findings of the E39/C time-slice experiments (Hein et al., 2001). However, in the Southern Hemisphere the model shows an improved behaviour with regards to former studies with E39/C: The absolute total ozone values are in overall agreement with TOMS, merely the ozone hole season last a little bit longer and the mid-latitude ozone maximum is somewhat higher. This model improvement can partly be reduced to the fact that large SZAs are now considered for the calculation of photolysis rates which has a clear impact on the model behaviour, in particular in the Southern Hemisphere (see below and Lamago et al., 2003). Currently it is not clear what the reasons are for the hemispheric differences in absolute accuracy of total ozone.

Figure WP4-2d displays the differences of the two model climatologies (Figs. WP4-2a and WP4-2b), to illustrate the calculated ozone changes in E39/C during the simulated episode. Since the 1960s and 1970s represent a climatological mean state of an almost unperturbed episode, this climatology (Fig. WP4-2a) can be taken as a basis to derive trends from 1980 onwards. The difference between the 1980s and 1990s climatology (Fig. WP4-2b) to the unperturbed climatology (Fig. WP4-2a) represents then the decadal trend (Fig. WP4-2c). As anticipated, largest changes are found in the south polar region, where 60 DU less ozone is calculated in the second half of the transient simulation compared with the first half. This is about 25% per decade. Especially in the 1990s, ozone decreases steadily with 30 to 40% less ozone at the end of the century compared to 1980. These trends agree well with observations. For example, based on TOMS-data for the years between 1978 and 1994, McPeters et al. (1996) estimated the ozone loss to be 20%/decade.

In the Northern Hemisphere, the trend pattern and absolute numbers agree with analyses from measurements: McPeters and colleagues found an ozone reduction in northern spring of about 6%/decade. The model shows a decrease of about 25 DU (Fig. WP4-2d), which relates to a trend of 5% per decade. A small increase (less than 7 DU) in total ozone is simulated by E39/C in northern summer. It is caused by an increase of tropospheric ozone concentration whereas at the same time no clear change is simulated in the lower stratosphere. The vertical ozone distribution (not shown) and its seasonal changes are in reasonable agreement with observations (Fortuin and Kelder, 1998). The simulated ozone changes throughout the four decades are almost statistically significant: Ozone mixing ratios have increased during equinox (MAM, SON) in the Northern Hemisphere middle troposphere by more than 10 ppbv, whereas in the lower stratosphere an obvious general decrease is found, in particular in the polar Southern Hemisphere spring time.

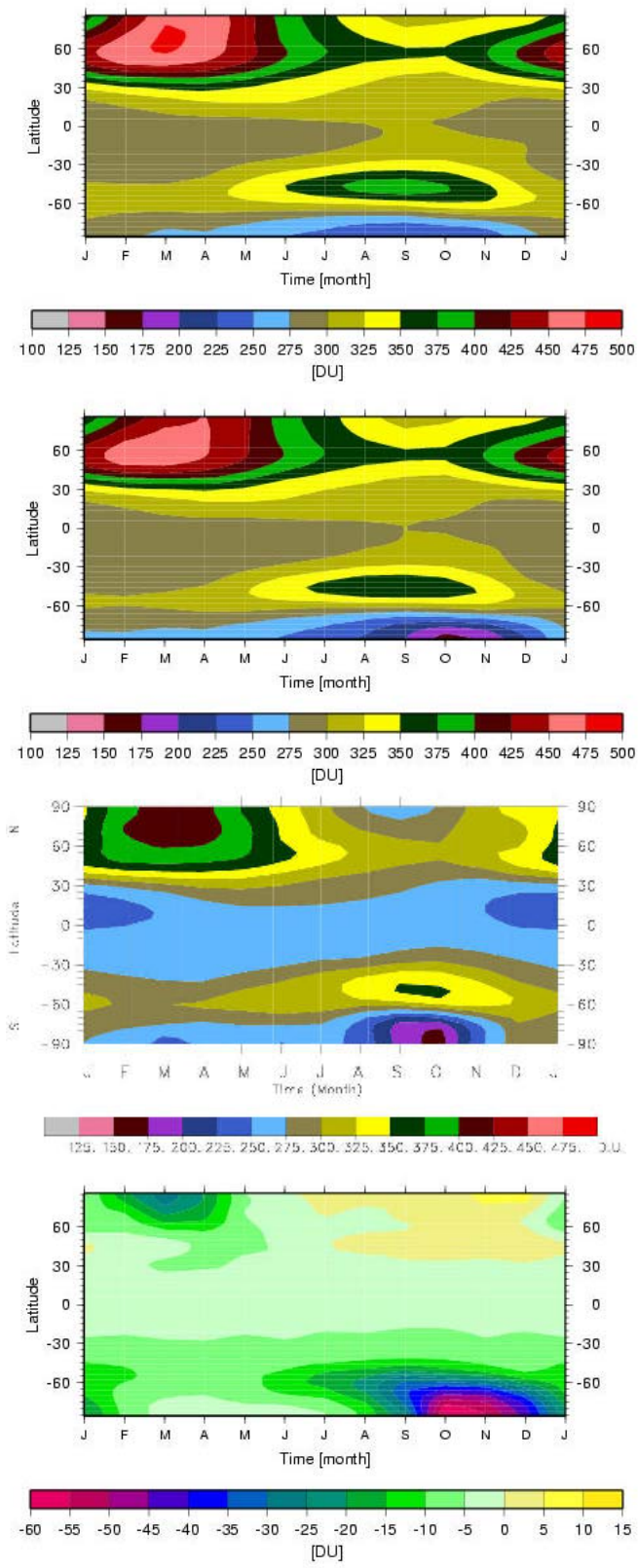

Figure WP4-2: Climatologies of total ozone (in Dobson Units) derived from E39/C transient run for 1960 to 1979 (uppermost top), E39/C for 1980 to 1999 (second top), TOMS for 1985 to 1997 (third top). Lowermost panel shows the differences between the two E39/C climatologies. Negative (positive) values (in Dobson Units) indicate lower (higher) total ozone in the years between 1980 and 1999.

To get a closer insight into the regionally change pattern and the inter-annual variability of ozone changes, Figure WP4-3 shows total ozone anomalies for the whole model simulation with respect to mean values based on the years 1964 to 1980. The features discussed above can easily be identified again, especially that the ozone depletion starts first in high latitudes of the Southern Hemisphere and that the reduction of the ozone layer is delayed in the Northern Hemisphere and the tropical region. But there are also some additional extraordinary features which are eye-catching: For example, as identified in observations (Bojkov and Fioletov, 1995), the ozone holes (i.e., the area covered by total ozone values less than 220 DU) in the years 1986 and 1988 are clearly smaller than in the respective year before. A closer inspection of the dynamics of the polar vortices in E39/C during these years indicate in both cases a mid-winter warming of the polar lower stratosphere along with a displacement of the polar vortex towards lower latitudes, which is very similar to the observed dynamic behaviour of the polar vortices in 1986 and 1988. There are a number of other interesting similarities in mid-latitudes of the Southern Hemisphere, i.e., positive an negative ozone anomalies which nicely match in observations and results from the transient run, in particular in 1985, 1989, 1991/92, and 1996 (see Bojkov and Fioletov, 1995, their Plate 1). A comprehensive discussion about possible reasons for these consistencies with observations will be given in the next section. Looking into the tropics, the variability of total ozone is also conspicuous, which notedly reflects the QBO signal.

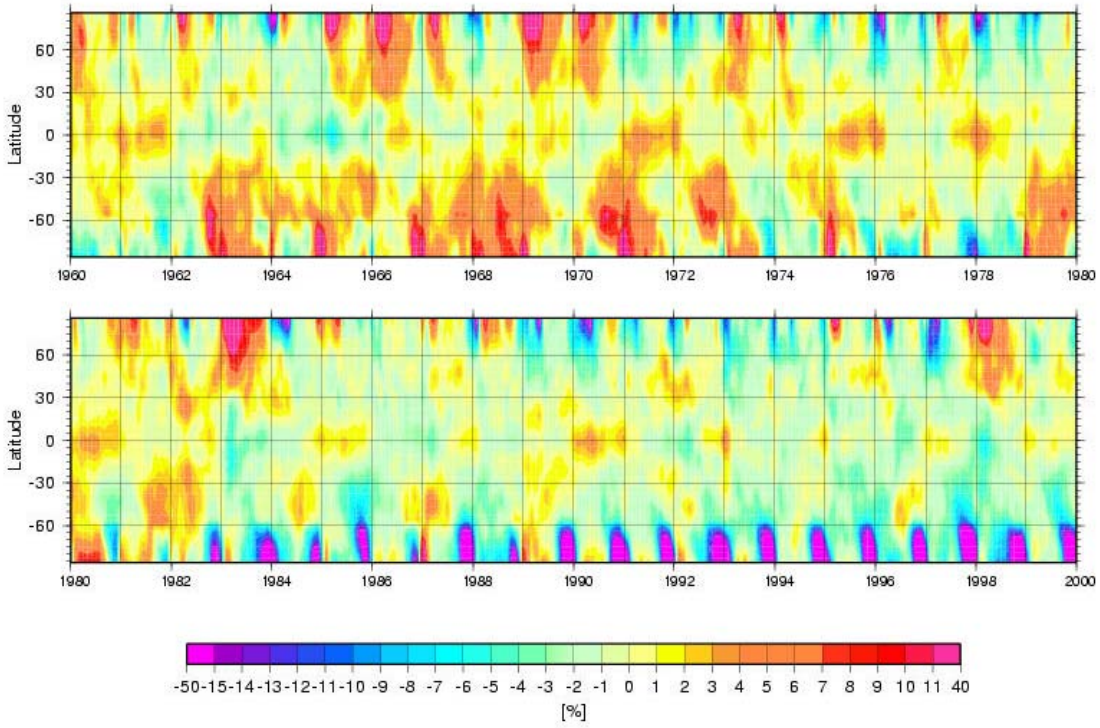

Figure WP4-3: Anomalies of total ozone (in percent) derived from the E39/C transient simulation. Anomaly values are calculated with respect to mean values of 1964 to 1980.

Temperature and zonal wind

Climatologies of temperature and zonal mean wind fields for the 1960s and their changes throughout the four decades, as simulated by E39/C, are displayed in Figures WP4-4 and 4-5. The mean fields (Figs. WP4-4a and 4-5a) are satisfactorily reproduced compared with observations (e.g., re-analyses of the European Centre for Medium Range Weather Forecasts). Sub-tropical and polar night jets are clearly distinguishable, i.e., a transition zone with reduced wind speed is found in both hemispheres for all seasons. A continuous model problem arises in the Southern Hemisphere winter months (JJA), where E39/C is calculating too low temperatures in the polar lower stratosphere (below 180 K). Therefore, the climatological mean polar vortex is too strong and stable (Fig. WP4-5a, see also Hein et al., 2001; Austin et al., 2003). Another discrepancy has been identified in the zonal mean stratospheric wind fields in the summer hemispheres. The summer vortices in both hemispheres are slightly shifted

towards the tropics, which leads to an insufficient wind reversal at higher latitudes. No easterlies winds are simulated poleward of 55°S in the Southern Hemisphere (DJF) and in the Northern Hemisphere (JJA), the calculated easterlies at polar latitudes are too weak. The structure of temperature changes between the 1960s and 1990s mostly arises from the increase in greenhouse gas concentrations (i.e., increase of tropospheric temperature, decrease of stratospheric temperature), but also reflects the ozone changes (Fig. WP4-4b). Strongest temperature decreases are seen in the Southern Hemisphere polar lower stratosphere in SON (up to -10 K at 30 hPa) and DJF (up to -6 K at around 70 hPa), the time during and after the appearance of the ozone hole. A statistically significant temperature increase of more than 1 K is found in the (sub-)tropical upper troposphere and middle and higher latitudes of the Northern Hemisphere lower and middle troposphere. Corresponding changes of the zonal mean wind field are shown in Fig. WP4-5b. The statistically significant increase of the zonal mean wind speed of up to 6 m/s in the Southern Hemisphere lower stratosphere during spring (SON) and summer months (DJF) can directly be related to the ozone hole and the corresponding decrease of stratospheric temperatures. Another systematic change pattern which is obvious throughout all seasons, is found in mid-latitudes of the Northern Hemisphere. Here, the temperature change in the upper troposphere / lower stratosphere increases the horizontal temperature gradient, which intensifies the zonal wind due to the thermal wind equation. This results in a more intense jet stream in DJF and MAM, and tends to shift the jet stream to lower latitudes in JJA and SON. This is accompanied by a warming of the northern polar region and a reduction of the horizontal temperature gradient at lower altitudes, resulting in a reduction of the zonal mean wind at around 50° to 60°N.

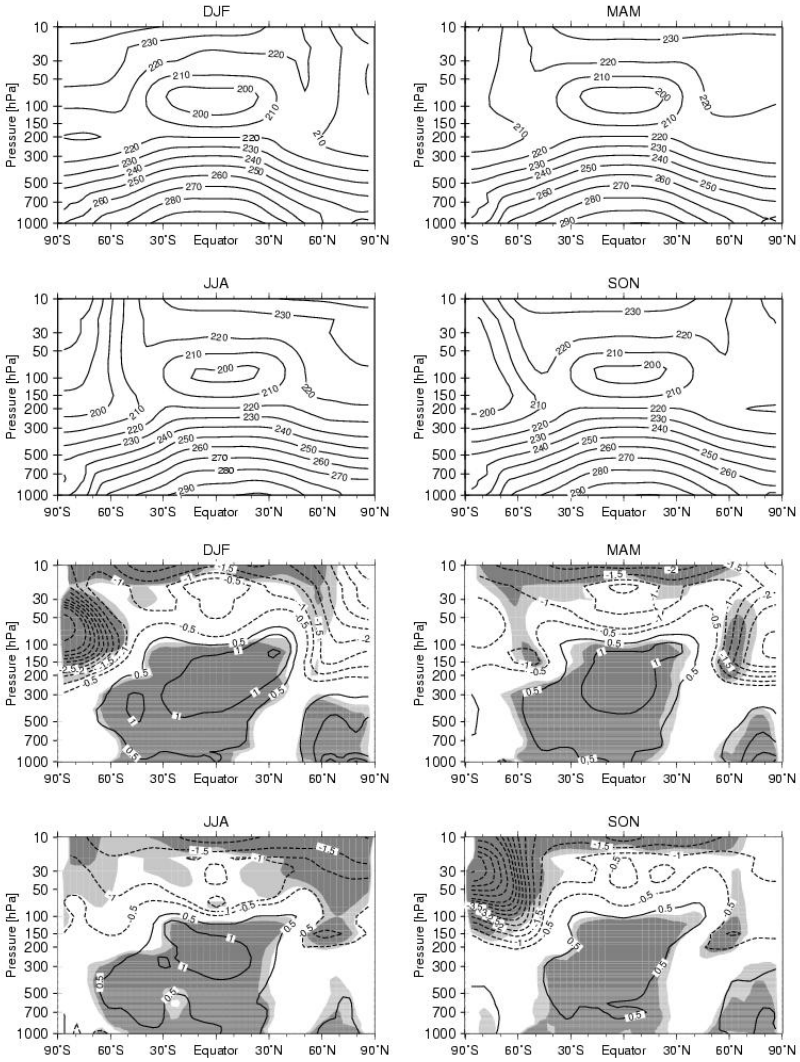

Figure WP4-4: (a) Seasonal means of zonal mean temperatures (in K) derived fron the E39/C transient simulation for the 1960s (top four figures). (b) Differences of seasonal means of zonal mean temperatures (in K) between the 1960s and the 1990s. Positive (negative) values indicate a warming (cooling) from the 60s to the 90s. Dark (light) shaded areas indicate the 99% (95%) significance level (t-test).

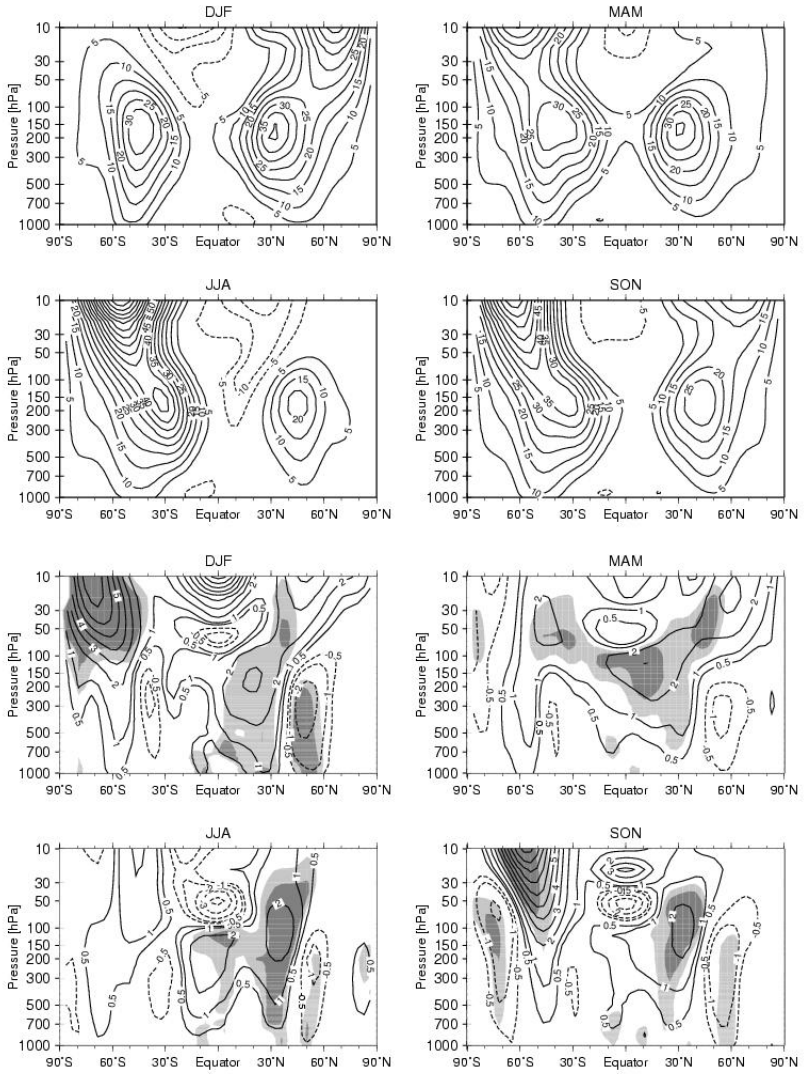

Figure WP4-5: As Fig. WP4-4, but for the zonal mean wind (in m/s).

To display dynamic changes during the 40 model years, an analysis of zonal mean temperature and zonal wind is presented in the style of the NCEP analyses. Figure WP4-6 shows climatological mean curves of the annual cycle of the zonal wind at 60°N and S at 30 hPa (Figs. WP4-6a and 4-6c) and of the zonal mean temperature at 80°N and S at 30 hPa (Figs. WP4-6b and 4-6d). The different lines represent mean values for the four decades covered by the transient simulation, the shaded area denotes the minimum and maximum values reached during the 1960s of the model. Similar to the results presented in Hein et al. (2001), the model shows it ability to reproduce hemispheric differences with regards to dynamic variability. Although the annual cycle is well captured in both hemispheres, and the mean values in the Northern Hemisphere agrees well with respective analyses derived from observations (see NCEP web-page), the model offers some deficiencies in the Southern Hemisphere: Polar temperatures are too low in winter (JJA), and the wind reversal (easterlies) during summer time (DJF) is not simulated at this latitude and altitude. This reflects the well-known cold-pole problem ("cold bias") which mostly all CCMs and GCMs have in common and which has been intensively discussed in Austin et al. (2003). With regards to the dynamic variability of the Northern Hemisphere during winter and spring, E39/C shows a weaker inter-annual variation only in early winter time. Obviously, E39/C is able to reproduce stratospheric warmings. In both hemispheres, the winters of the 1960s are the warmest and the zonal mean winds in late winter and spring are weaker than for the other decades. Whereas the climatological mean values for the other decades do not indicate a systematic changes in the Northern Hemisphere (mainly due to the high dynamic variability), the zonal mean zonal wind and temperature in the Southern hemisphere do steadily change to stronger

(more stable) polar vortices and colder conditions in late winter and early spring. The lifetime (persistence) of the polar vortex has been elongated by about three weeks. This is in good agreement with an estimate presented by Zhou et al (2000) who carried out their analysis on 19 years (1979-1998) of NCEP/NCAR reanalysis data and found that the Southern Hemisphere polar vortex has lasted about two weeks longer in the 1990s than in the early 1980s.

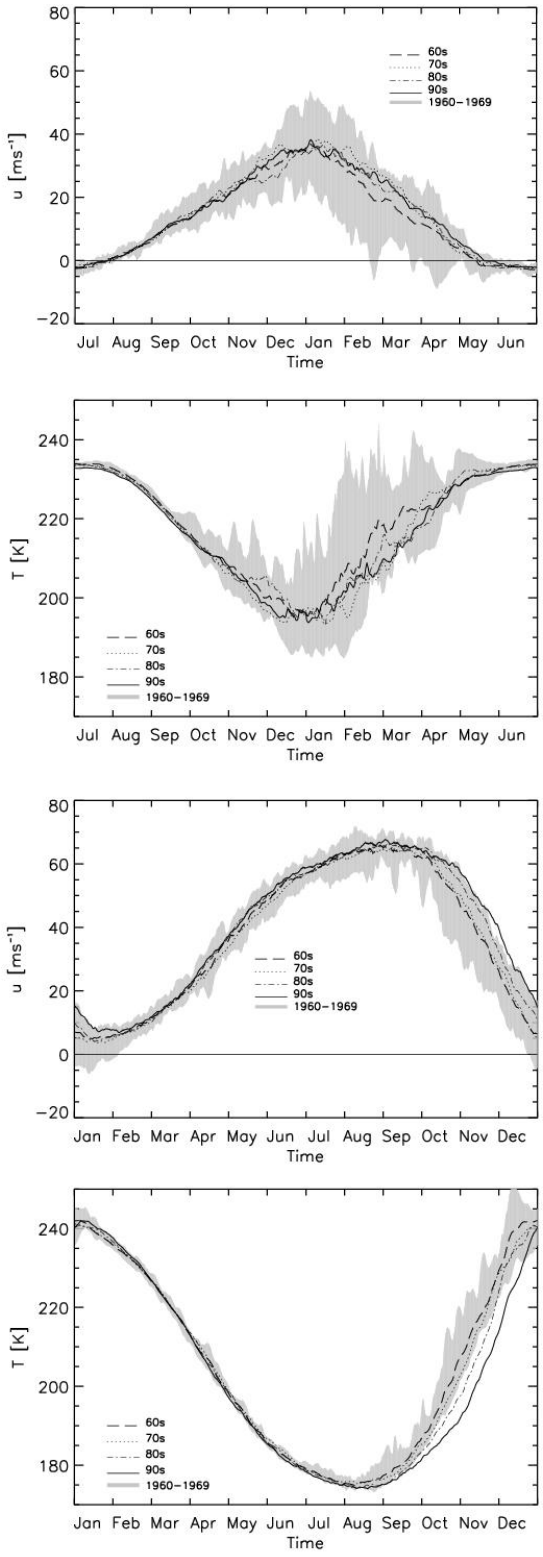

Figure WP4-6: Results of E39/C transient simulation. (a): Seasonal changes of zonal mean wind (in m/s) at 60°N (uppermost top), (b): of zonal mean temperature (in K) at 80°N (second top), (c) of zonal mean wind at 60°S (third top), and (d) of zonal mean temperature at 80°S, all at 30 hPa. Lines denote decadal averages, the shade indicates the area of min/max values during the 1960s.

Tropopause and water vapour

It is still under debate if there is a significant trend towards higher water vapour concentrations in the (lower) stratosphere, and about possible mechanisms driving these changes. One problem is that analyses of different time series of measurements do not result in a uniform picture, not even the sign of the change is clear (Randel et al., 2004). Although it was not in the focus of this project to investigate in detail the mechanisms responsible for long-term changes of water vapour concentrations in the lower stratosphere, in the following, a brief overview of relevant model results is presented.

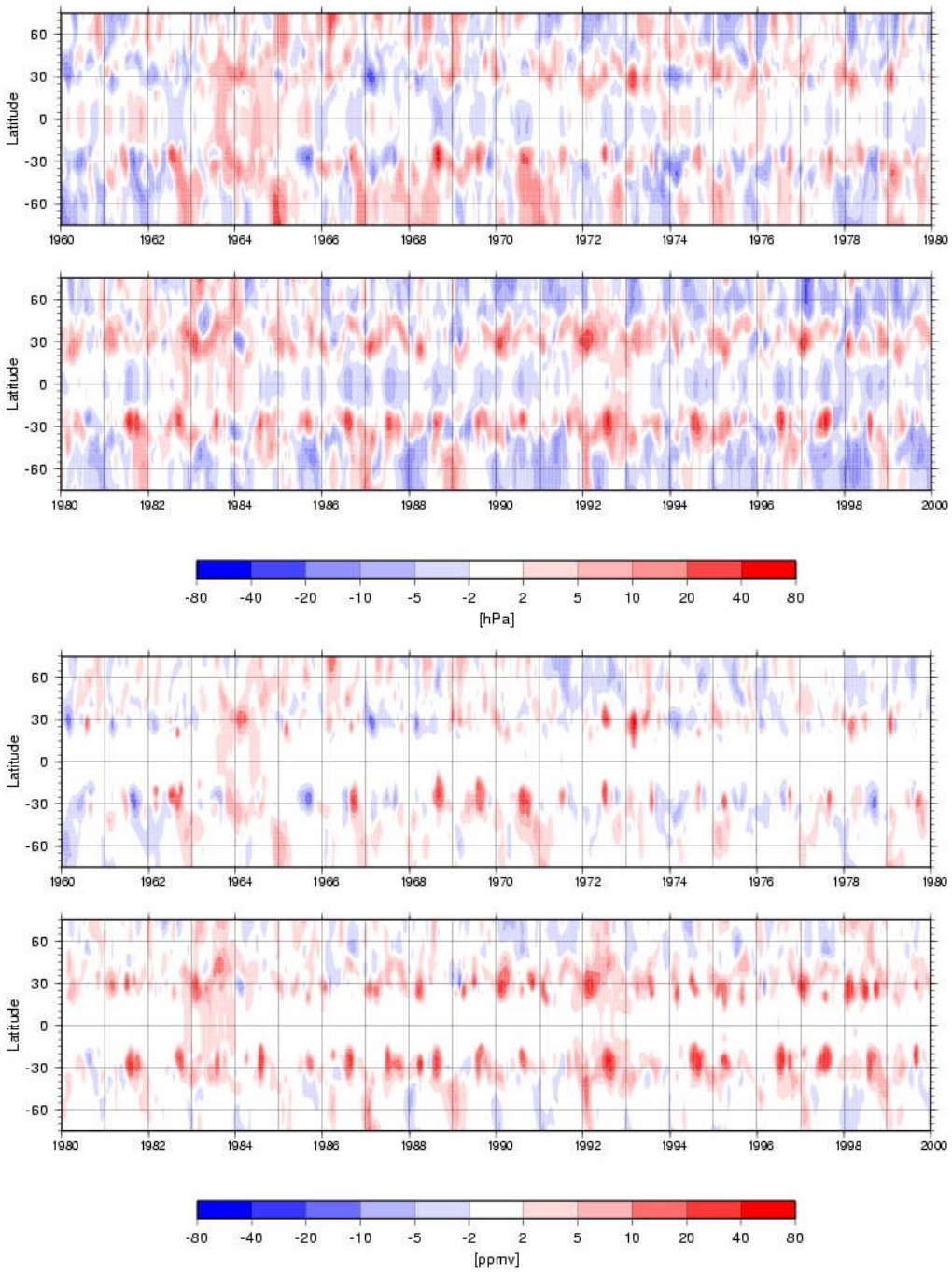

Figure WP4-7: (a) Anomalies of tropopause pressure (in hPa) derived from E39/C transient simulation (top) and (b) of water vapour mixing ratio (in ppmv) at the thermal tropopause, both with respect to mean values for 1964 to 1980.

The changes of the pressure of the thermal tropopause are given in Figure WP4-7a. Whereas no obvious systematic changes (trends) are seen in the first two decades of the transient simulation, the model results indicate a continuous change in tropopause height in subsequent years. In both hemispheres, E39/C simulates a decrease (increase) of tropopause pressure (height) poleward of around 50°. The subtropical regions show an increase (decrease) of tropopause pressure (height). No long-term changes can be detected in the tropics. The major volcanic eruptions considered in the transient simulation lead to a temporary increase of tropopause pressure. Changes in tropopause temperature (not shown) are directly related to the variability of the tropopause height: An increase (decrease) of tropopause height goes along with a decrease (increase) of tropopause temperature. A comparison with an analysis of tropopause height changes at 47°N (Steinbrecht et al., 1998; 2001) shows a qualitative agreement, i.e., a more or less steadily increase of tropopause height in February during the last 30 years. However, here the model is underestimating the rise in tropopause height. The analysis of Steinbrecht and colleagues (2001) gives +125 m/decade for the station Hohenpeissenberg, E39/C calculates +80 m/decade for the corresponding model grid point.

Figure WP4-7b depicts the changes of water vapour mixing ratio at the thermal tropopause during the 40 year model simulation. The clearest indication for a change is only found in the subtropical region, where the water vapour mixing ratios are obviously higher in the late 1980s and the 1990s. Systematic mutations in model results cannot be identified in the tropics and middle and high latitudes of both hemispheres. Again, the volcanic eruptions involve characteristic signatures (see below). Looking higher up into the lower stratosphere, a comparison with measurements of the Boulder frost point hygometer and corresponding HALOE data (Randel et al., 2004) is performed. The general distribution of the change pattern in the lower stratosphere is equal to that at the tropopause.

Further analysis of timeslice experiments with E39/C

A study has been made to investigate the reasons for enhanced planetary wave activity in E39/C in a future scenario calculation (Schnadt et al., 2002) which yield an accelerated recovery of stratospheric ozone in the Northern Hemisphere (Schnadt and Dameris, 2003). It has been shown that the model is able to reproduce the observed behaviour, i.e. that a positive NAO index corresponds to an anomalously strong polar vortex, while an anomalously weak polar vortex is found when tropospheric circulation anomalies are of the opposite sign. In E39/C the NAO index decreases significantly from "1990" to "2015". This coincides with enhanced vertical propagation of quasi-stationary waves and a dynamical heating of the northern polar stratosphere. Thus, tropospheric circulation changes might influence stratospheric dynamics and hence northern hemisphere ozone evolution. The results clearly illustrate the coupling of the troposphere and stratosphere and the importance of interaction of dynamical and chemical processes in the UTLS region.

Development of parameterisation of twilight conditions and implementation in E39/C

In a joint action with MPI-C, E39/C has been employed to assess the impact of solar zenith angles (SZAs) larger than 87.5° for the chemistry and dynamics of the lower stratosphere, in particular at polar latitudes during winter and spring. It is well-known that the impact of photolysis on mixing ratios of chemical species depends on the maximum SZA allowed in model calculations. For example, an estimate by the 2D chemistry model MPIC for a specific case study at the 475 K isentropic level showed that the total percentage ozone loss increased from 25% to 31% when the maximum SZA was raised from 90° to 92° (Krämer et al., 2003). Moldanova et al. (2002) showed that for some halogenated species and NO_3, the photolysis beyond 90° SZA may be of importance. Nevertheless, some CCMs neglect the impact of twilight for simplicity reasons, which certainly has an impact on chemical processes, especially during winter and spring near the edge of the polar night. The investigation carried out in this study has aimed to quantify the effect of photolysis beyond 87.5° SZA in a fully coupled 3D CCM. A brief description of the employed model system E39/C and a detailed explanation of the newly developed parameterisation for the photolysis up to 93° SZA has been given by Lamago et al. (2003). Results of a E39/C simulation considering SZAs up to 93° with those of a sensitivity run with SZAs confined to 87.5° has been compared. A comprehensive summary is given in the following.

Figure WP4-8 shows the differences between the modelled climatological mean total ozone fields (SZA93 minus SZA87.5). In the southern mid- and high latitudes between 30°S and 90°S the largest ozone difference values are simulated. These differences are statistically significant due to the relative low inter-annual variability. The ozone reduction is strongest south of 60°S between September and November due to the photon surplus in SZA93. The maximum differences are found in the centre of the polar vortex. At the end of September approximately 30 Dobson Units (DU) less ozone is found in the SZA93 case. This corresponds to a maximum reduction of the ozone column over the south polar region of about 20% in the SZA93 run in comparison to the SZA87.5 simulation. A closer inspection indicates that in the SZA93 simulation ozone depletion starts earlier. Statistically significant temperature differences between the SZA93 and the SZA87.5 simulations are mainly found in the extra-tropical Southern Hemisphere lower stratosphere (between 10 and 100 hPa). Figure WP4-9 shows the differences for the 50 hPa pressure level. The largest values occur during polar spring (up to –4 K) indicating that the SZA93 simulation produces colder conditions there. Near the edge of the Southern Hemisphere polar vortex the SZA93 run shows a cooling between –0.5 K and –1 K. These temperature differences can be easily related to the detected changes of the ozone column between the two model runs (Fig. WP4-8). In SZA93, the stratosphere is colder in regions with reduced ozone columns with regards to the SZA87.5 run. Temperature differences in the Northern Hemisphere are statistically not significant due to the high dynamic variability especially in winter and spring time.

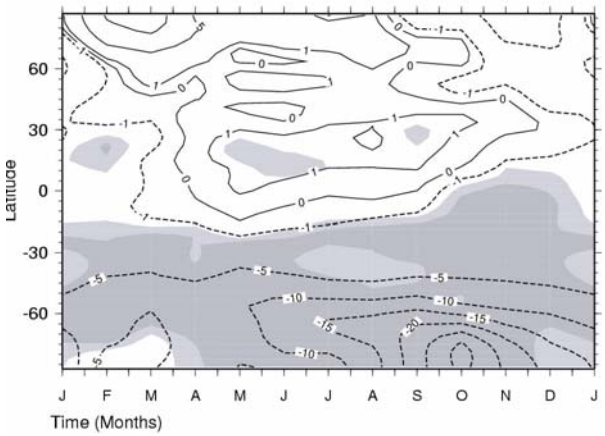

Figure WP4-8: Changes in total ozone (in DU) between the model simulations SZA93 and SZA87.5. Negative (positive) values indicate lower (higher) values in SZA93. Dark (light) shaded areas indicate the 99% (95%) significance level (t-test).

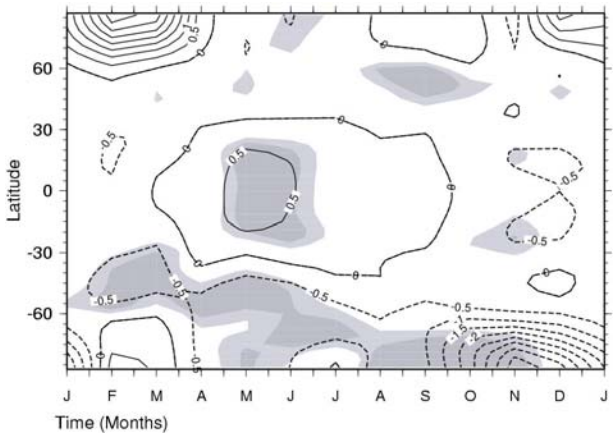

Figure WP4-9: Changes of climatological mean temperature (K) at 50 hPa between the model simulations SZA93 and SZA87.5. Negative (positive) values indicate lower (higher) values in SZA93. Dark (light) shaded areas indicate the 99% (95%) significance level (t-test).

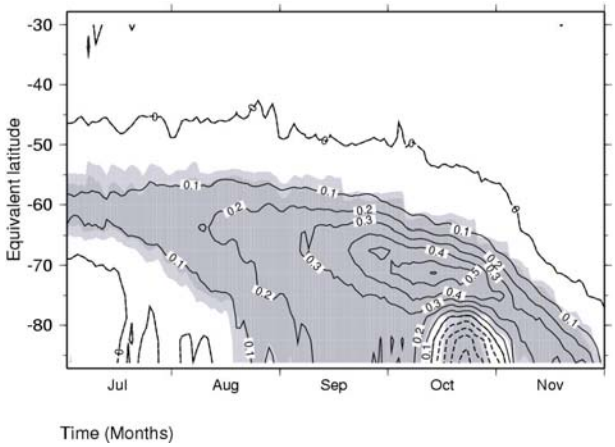

Figure WP4-10: Changes of the climatological zonal mean for ClO_x (ppbv) at 50 hPa in the Southern Hemisphere between the simulations SZA93 and SZA87.5. Model data have been transformed to the PV-coordinate system. Positive (negative) values indicate higher (lower) values in the SZA93 simulation. Dark (light) shaded areas indicate the 99% (95%) significance level (t-test).

To estimate the importance of considering SZAs greater than 87.5° on stratospheric chemistry in a fully coupled 3D CCM, some chemical species have been analysed which are especially relevant for

polar chemistry. The diagnostics have been concentrated on the Southern Hemisphere. As shown above, stratospheric temperatures are reduced if SZAs up to 93° are considered, especially in springtime inside the polar vortex. This favours the formation of PSCs in the SZA93 run. In this region the conditions are most favourable for heterogeneous chemistry on PSC surfaces during the polar night. Figure WP4-10 shows the differences in ClO_x at the 50 hPa pressure level. An enhanced activation of chlorine is found inside the polar vortex between July and November. Maximum difference values are about 0.5 ppbv, these differences are statistically significant. An exception is found inside the polar vortex in the second half of October where a decrease of ClO_x (up to –0.3 ppbv) is detected in the SZA93 run. This behaviour can be explained considering the related differences of $ClONO_2$ and HCl (see Lamago et al., 2003). Reduced $ClONO_2$ mixing ratios are found in the SZA93 run inside the polar vortex between mid October and mid November while HCl is increased there. Although the results of both simulations SZA93 and SZA87.5 show a realistic behaviour with regards to the re-formation of the chlorine reservoirs, i.e., ClO_x is first converted towards HCl, the SZA93 simulation produces improved results concerning the re-formation (2 weeks earlier), which means that they are closer to the analyses of observations.

This study was the first assessment using a 3D CCM to quantify the effects of high SZAs on the dynamics and chemistry of the lower stratosphere. It shows that the photolysis for SZAs greater 87.5° is relevant especially in polar regions and cannot be neglected for simplicity reasons as partially done in other CCMs (e.g., Austin et al., 2003). Therefore, the parameterisation of photolysis frequencies at large SZA developed here will be a component of future studies with E39/C.

Joint contribution of MPI-MIPS and MPI-C

Coupling of the sulphate aerosol model (SAM) with MAECHAM/CHEM

In close cooperation, MPI-C and MPI-MIPS have coupled the global stratospheric aerosol model SAM (Timmreck, 2001) which explicitly calculates microphysical processes (nucleation, condensation, coagulation, sedimentation) with the MAECHAM4/CHEM (Steil et al., 2003). In this context SAM has been substantially revised. A new parameterisation of the homogenous nucleation rate (Vehkamäki et al., 2002) for upper tropospheric and lower stratospheric conditions and a new fit functions for the aerosol density have been implemented in the model system. In addition, COS and H_2SO_4 has been introduced as new tracers. COS is prescribed at the surface assuming a seasonal cycle with an average mass mixing ratio of 530 pptv for the Northern and a constant mass mixing ratio of 485 pptv for the Southern Hemisphere. CHEM has been extended with a stratospheric sulphur scheme (chemical reactions rates and photolysis rates of COS, SO_2, SO_3 and H_2SO_4). The aerosol surface area densities are estimated directly in the coupled microphysical model instead of being prescribed by a global and zonal constant surface area distribution. The aerosol number density is now taken into account in the calculation of the actinic flux in the photolysis routine. In the original version of the photolysis routine a mixture between rural and maritime aerosol is assumed for the aerosol number density, which is then vertically interpolated. Now the simulated aerosol number density is added to the background number density.

Figure WP4-11 shows the occurrence of new particle formation in the UT/LS region. Although the amount of the H_2SO_4 concentration influences the strength of the nucleation, the occurrence of the homogeneous nucleation is mainly determined by the temperature. Hence, the formation of new particles through homogeneous nucleation takes place preferably in the tropics around 17 km, where the coldest temperatures in the model occur and at the winter poles.

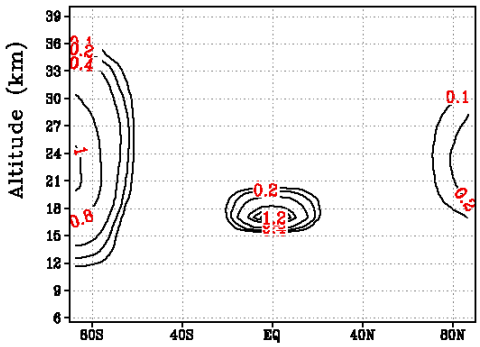

Figure WP4-11: Annual averaged binary homogenous nucleation rate (cm^3 s^1) in the coupled model run.

Contribution of MPI-MIPS

Implementation of SAM in ECHAM5

In parallel, a Fortran90 version of SAM has been implemented into the ECHAM5. ECHAM5 is the latest version of the Hamburg climate model ECHAM which can be run in different vertical and horizontal resolution and on various platforms (e.g. supercomputers and PCs). A further advantage of ECHAM5 is that it can quite easily be run in a 1D version which allows a relative fast testing of parameterizations. The model can also be operated in a nudged mode and is therefore better suitable for a comparison with specific observations. For the implementation in ECHAM5 SAM is rewritten in FORTRAN90 and adopted to a modular structure. This should make a coupling with the PSC and chemistry modules from MPI-C quite easily. The following changes have been carried out with respect to the ECHAM4 version:

- 44 tracer representing aerosol size distribution instead of one,
- new nucleation scheme (Vehkamäki et al., 2002),
- wet deposition in dependence of aerosol radius,
- new dry deposition (L. Ganzeveld, MPI-C:, pers.com) for gases and aerosols depending on aerodynamic and boundary layer resistances and a high resolution ecosystem database.

A first multi-annual simulation has been performed in T21 resolution (Figure WP4-12) and is currently validated. For the near future simulations with a higher vertical and horizontal resolution are planned. In addition, a coupling with the PSC module from MPI-C is intended for autumn 2004 until then both modules should run independently.

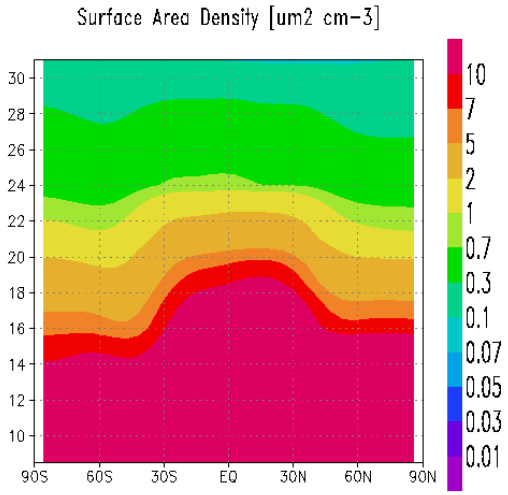

Figure WP4-12: Background aerosol simulation with ECHAM5/SAM in latitude-altitude cross section of the zonally averaged stratospheric aerosol surface area density. Annual mean of the third year of simulation.

First simulations of the CMCM comparisons with standard MAECHAM4

A first multi-annual run has been performed with the chemistry microphysics climate model (CMCM) MAECHAM4/CHEM/SAM. H_2SO_4 and COS were introduced as prognostic variables. The aerosol surface area densities were estimated directly in the coupled microphysical model instead of being prescribed by a global and zonal constant surface area distribution. The aerosol number density was taken into account in the calculation of the actinic flux in the photolysis routine. Sulphur chemistry was treated separately from the chemistry module CHEM.
The first results looked promising however the vertical gradient in the stratosphere turned out to be to strong. Homogeneous nucleation was strongly dependent of cold temperatures and had a maximum in the tropics around 16 km throughout the year and in high latitudes in polar autumn and spring. In the lower stratosphere the maximum number concentration was found in the tropics and strongly linked to homogeneous nucleation. In the upper troposphere highest particle concentration were found in Northern Hemisphere (NH) mid-latitudes in spring. The concentrations differed between land and ocean up to two orders of magnitude. The geographical distribution was similar as observed during the CARIBIC project (Hermann et al, 2003) with high particle number concentration in the upper troposphere in NH summer over the Arabian Sea and at mid-latitudes over Europe and lower values in the subtropics over the Middle East (Figure WP4-13). In NH winter the particle concentration showed a decrease over Europe in the upper troposphere towards higher latitudes. The values were however higher as observed in particular over Europe because an anthropogenic SO_2 emission data set from the mid 80ties had been used. For future simulations a new emission data set for the year 2000 will be applied. The chemistry scheme CHEM has been extended together with MPI-C with sulphur chemistry reactions. These coupling revealed unexpected difficulties on which we have worked a couple of months in close cooperation with MPI-C. At present, this model configuration is tested. The extension

of the binary H_2SO_4/H_2O system to a ternary $H_2SO_4/HNO_3/H_2O$ system has therefore been postponed until these tests will be finished.

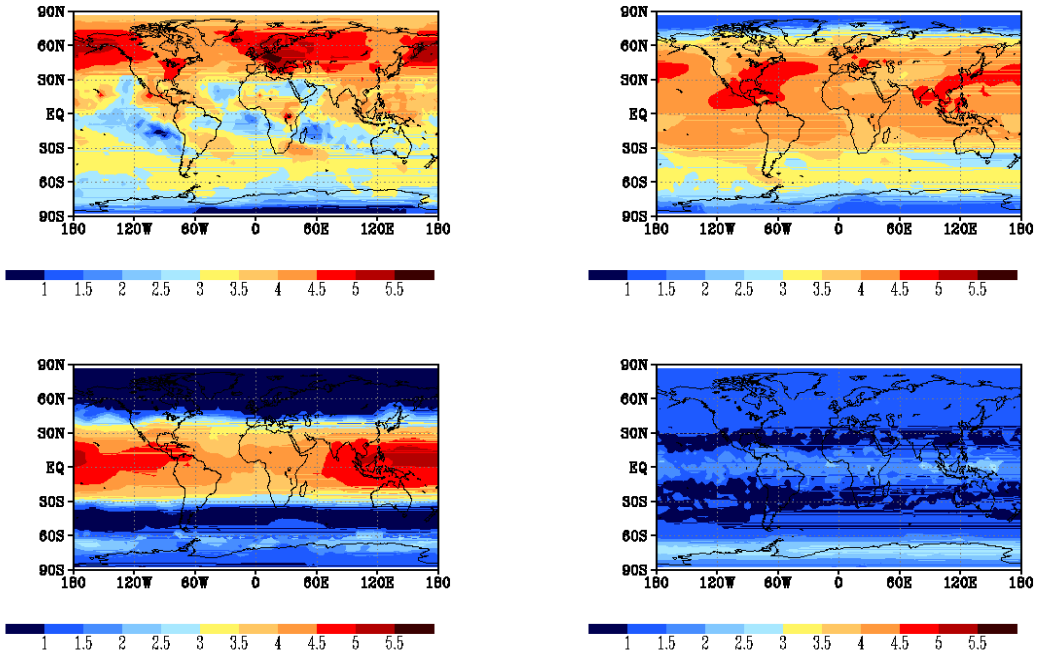

Figure WP4-13: Decadal logarithm of particle number concentration in JJA. The model results represent a five year average of a multi-annual simulation with the MAECHAM4/CHEM/SAM.

Joint contribution of FZJ and DLR

One of the main goals of KODYACS was to investigate the impact of the greenhouse effect on a future stratospheric chemistry. Although it seems that this may be accomplished by just studying the evolution of the chemistry of a CCM, there may be some differences between the atmospheric state, which is provided by the CCM, and the results of a highly resolved CTM with a more detailed chemistry and additional parameterised physical processes. Especially the effects of mixing, the existence of small-scale features with a considerable lifetime and the existence of NAT rocks may lead to a different chemical state of the atmosphere. It was therefore planned to do an offline-coupling between the E39/C (a CCM run by DLR) and the **C**hemical **La**grangian **m**odel of the **S**tratosphere CLaMS developed by FZJ.

To investigate the effects of the aforementioned (and other) processes on stratospheric chemistry, a preliminary CLaMS simulation driven by the dynamics taken from the E39/C 1990 timeslice experiment had been performed. This was meant to be a feasibility study concerning the technical aspects of coupling two models together and a case study as well. Because of its high resolution (50 km for this simulation) CLaMS is able to simulate small-scale mixing and to resolve filamentary structures from meteorological conditions provided by the CCM. The first results of a comparison considering methane as an inert tracer are shown in Figure WP4-14. Note that for the CLaMS simulation the tracer was initialised using results from the Mainz 2D model mapped onto equivalent latitudes. In addition to the large-scale features evident in both models, CLaMS reveals filaments of methane-rich air which are mixed into the polar vortex from mid-latitudes and persist for weeks. We expect this small-scale variability within the vortex to have a significant effect on ozone chemistry and estimates of future ozone loss.

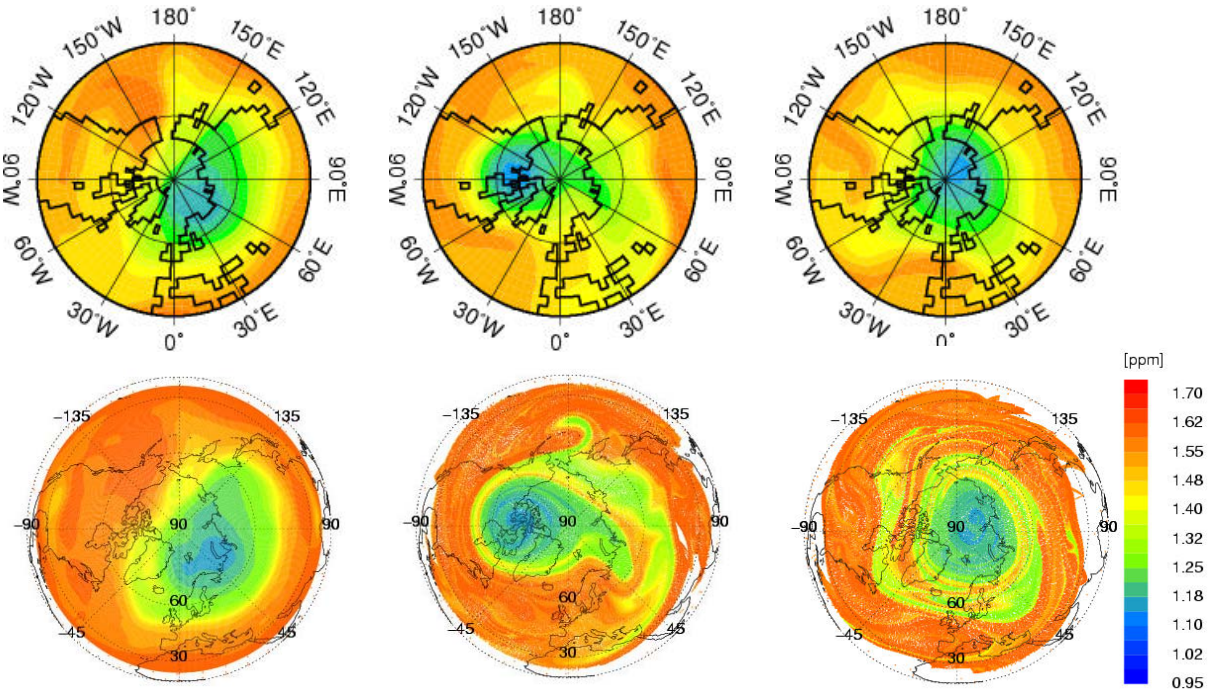

Figure WP4-14: Methane on the 475 K isentropic surface on January 1, 16 and 30 (left to right) taken from the 1990 timeslice experiment (year 43) of E39/C (upper panel). Results from a CLaMS simulation with the same background dynamics are shown in the lower panel.

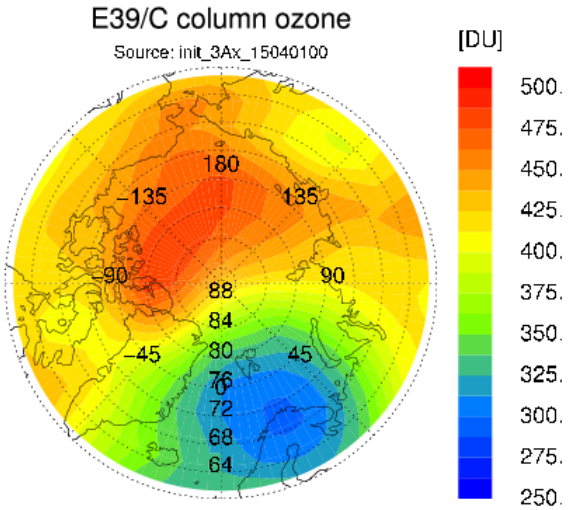

Figure WP4-15: Total Ozone in DU on April 1st, 2015, as simulated with CLaMS (initialisation by E39/C).

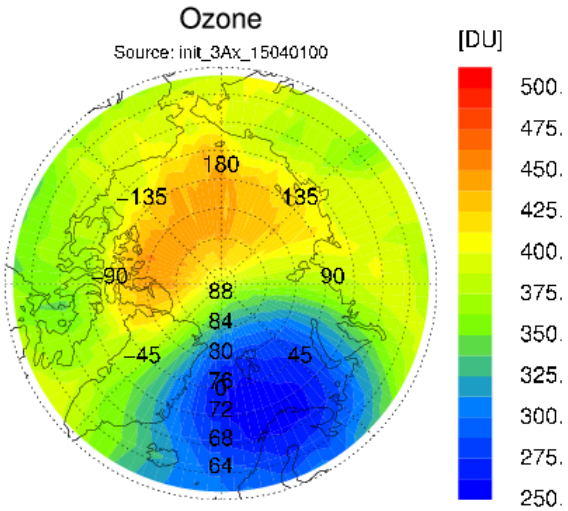

Figure WP4-16: Total Ozone in DU on April 1st, 2015, as simulated with E39/C.

During the next phase of the project the model runs based on the time slice experiments were extended to the time slice of 2015. GCM-simulated ozone loss for the time slice experiments '1990' and '2015' were determined with a methane-ozone correlation obtained on the 1st of January. For the winter with the largest ozone loss on the 475 K isentropic level (simulated winter 2015/58), multi-level and sensitivity studies were performed. Figure WP4-15 shows the ozone column simulated by CLaMS based on the CCM initialisation. Very low ozone column values (minimum value 268 DU) occur on the 1st of April in an area limited by 60°N to 80°N latitude and 20°W to 50°E longitude. These values are significantly lower than minimal ozone values simulated by E39/C as displayed in Figure WP4-16 and reported in WMO (2003). The minimum values for total ozone in the arctic spring of this simulation in E39/C are around 296 DU. The respective simulation carried out with CLaMS predicts a minimum ozone column of only 268 DU. The chemical ozone loss of this winter amounts to about 25 % (49 DU) of the total ozone reduction in the arctic stratosphere. In a scenario which includes bromine chemistry and denitrification CLaMS predicts a minimum in total ozone of about 235 DU, the contribution of chemical loss increases to 35 % (65 DU, see Figure WP4-17).

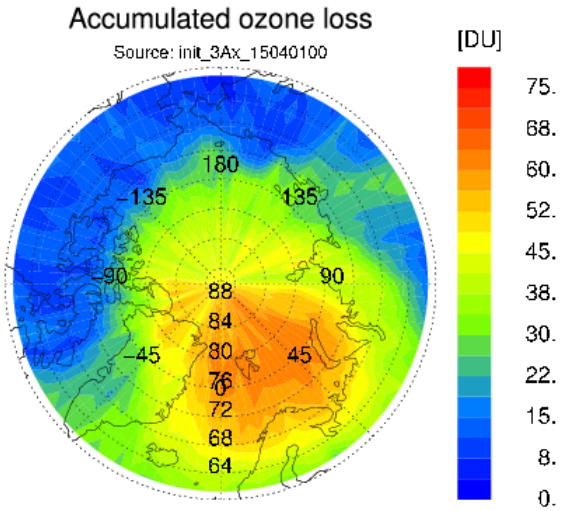

Figure WP4-17: Maximum chemical ozone depletion in DU as simulated by CLaMS, considering a height range between 350 and 550 K. This simulation was carried out with full chemistry including bromine.

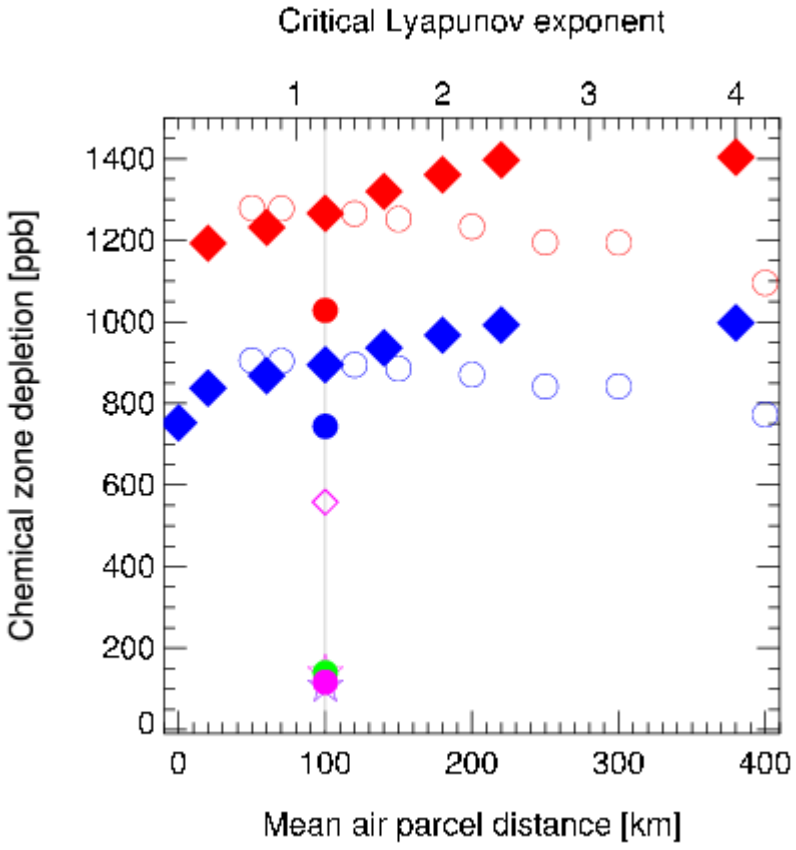

Figure WP4-18: Sensitivity of chemical ozone loss (in ppb) as predicted by CLaMS from parameters like resolution and mixing intensity, as well as to different chemical regimes like full chemistry with bromine (red), without bromine (blue), without denitrification (big circles), and without heterogeneous reactions (stars). See text for details.

To identify the underlying reasons for the discrepancy in simulated ozone loss, sensitivity studies for different mixing parameters, model resolutions and chemistry set-ups were performed. Figure WP4-18 shows for a number of simulation set-ups the 90-day accumulated ozone loss (in ppbv) on the 475 K isentropic surface in winter 2015/58. The initial resolution was varied between 50 and 400 km (lower axis in Figure WP4-18), the mixing intensity was tuned over a range of critical Lyapunov exponents

(upper axis, see Konopka et al., 2003). While mixing is the more important parameter for ozone loss, even with very strong mixing the chemical ozone loss predicted by CLaMS is much higher than in the E39/C results (indicated by the pink open diamond).

Reduced ozone loss in the sensitivity studies were attributed to increased deactiviation of active chlorine species to the reservoir species chlorine nitrate. This sensitivity and the underestimation of ozone loss (total column and volume mixing ratio) in previous CCM studies point to overestimated numerical diffusion in E39/C, which would import nitrous oxides from middle latitudes into the polar vortex, thus leading to early deactivation. The excess formation of chlorine nitrate can easily be seen by comparing the Figs. WP4-19 and 4-20, which display the horizontal distribution of $ClONO_2$ on the 475 K isentropic level on April 1st, 2015, simulated by CLaMS (Fig. WP4-19) and E39/C (Fig. WP4-20).

Please note the differences concerning the interior of the polar vortex, which is free of chlorine nitrate in the CLaMS atmosphere and shows high values in the E39/C atmosphere, and the formation of fine scale structures in the former case, which are eroded due to numerical diffusion in the latter.

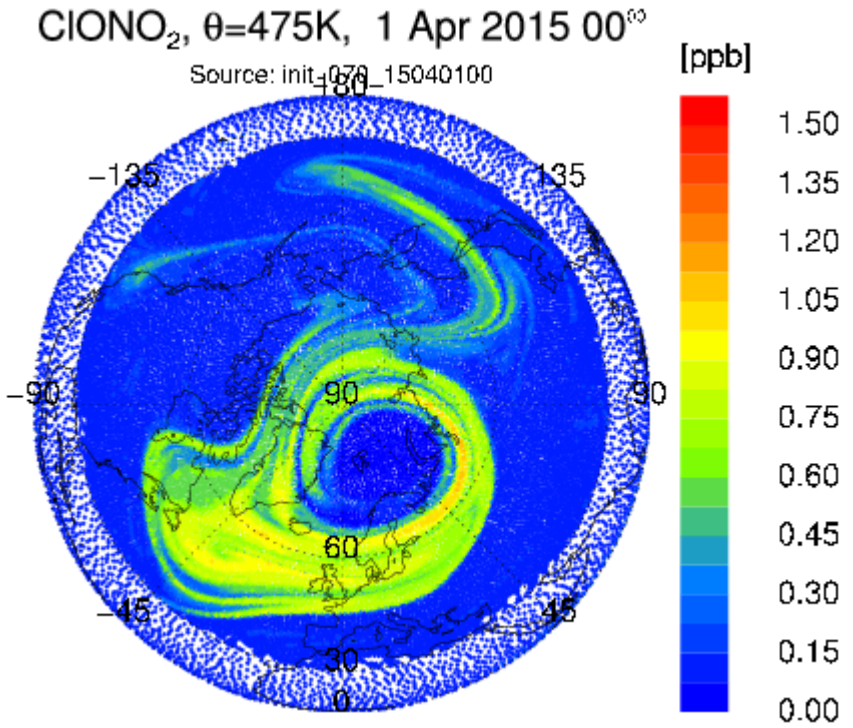

Figure WP4-19: Horizontal distribution of chlorine nitrate on the 475 K isentropic surface as for April 1st, 2015, as simulated by CLaMS.

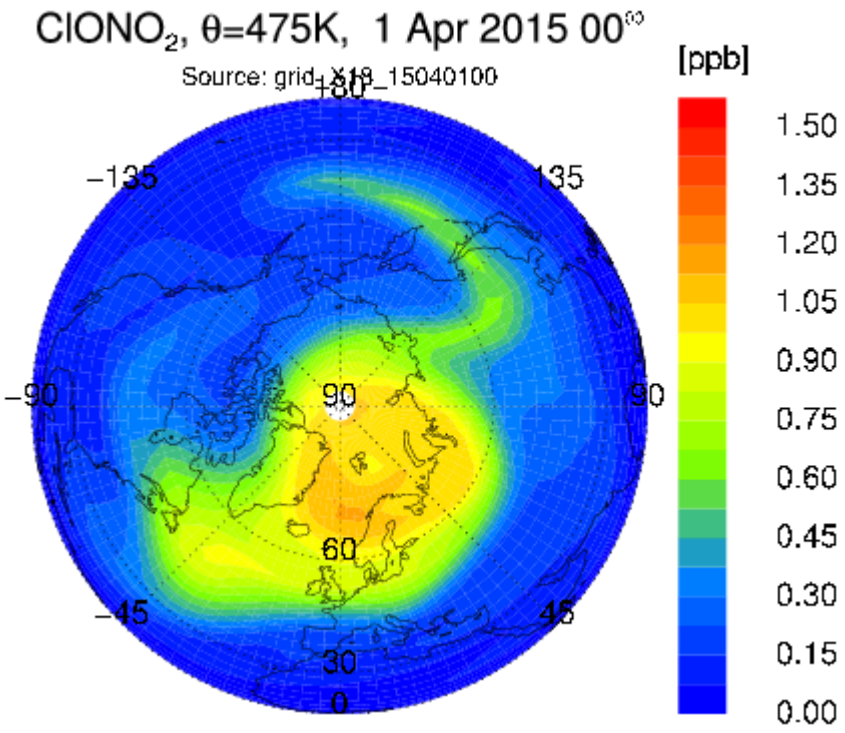

Figure WP4-20: Horizontal distribution of chlorine nitrate on the 475 K isentropic surface as for April 1st, 2015, as simulated by E39/C.

To differentiate chemical ozone loss from dynamical change in ozone, the tracer-tracer correlation technique (e.g. Tilmes et al., 2004) was applied to E39/C and CLaMS simulated methane and ozone fields. The correlation between these two species is established on the January data set supplied by E39/C, thus forming the early winter reference correlation. This reference correlation was used to calculate an expected spring ozone value. The difference between the expected and the simulated quantity of ozone is supposed to yield chemical ozone change.

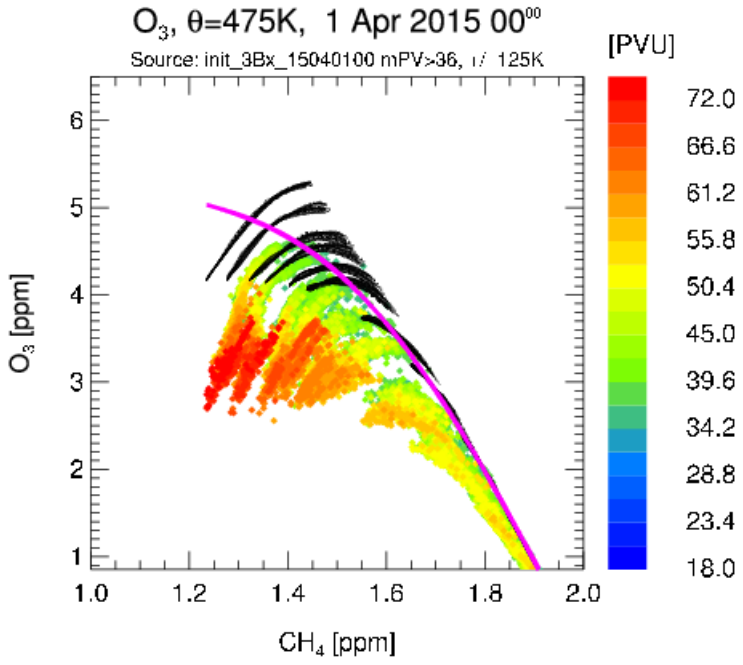

Figure WP4-21: Methane-ozone correlation in the polar vortex on the 475 K isentropic surface for spring as simulated by CLaMS. The early winter reference correlation is shown as a pink line. The colour code refers to the PV of the considered air parcels.

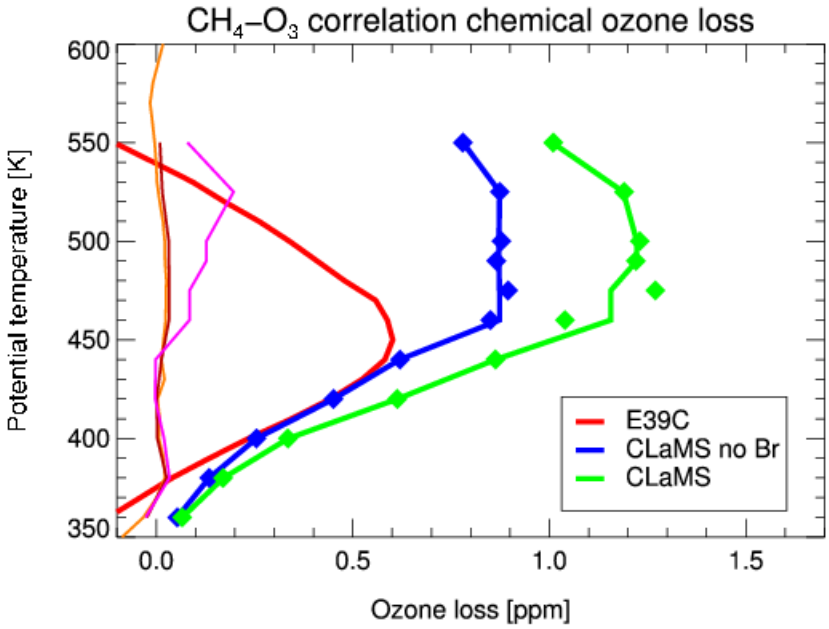

Figure WP4-22: Vertical profile of chemical ozone loss derived from the methane-ozone correlation (see Fig. WP4-21) for E39/C (red) and CLaMS with full chemistry (green) and without bromine (blue). Accumulated ozone loss derived from a passive ozone tracer within CLaMS (corrected for changes in the tracer correlation) is shown with diamonds.

Figure WP4-21 shows both, the early winter correlation (displayed as a pink line) between methane and ozone, and the correlation on April 1st, 2015, for all CLaMS air parcels on the 475 K isentropic surface. The colour code shows the value of Potential Vorticity of the air parcels, thus indicating their position with respect to the centre of the polar vortex. The ozone depletion caused by chemistry is now clearly visible as the difference between spring ozone and the early vortex correlation at a given methane value. Strongest depletion takes place inside the lower stratospheric vortex core with values well above 1 ppmv. Even in the vicinity of the vortex edge (indicated by lower PV values) substantial ozone loss can be observed.

The vertical profiles of ozone loss inside the vortex for all simulations are shown in Figure WP4-22. While below 450 K the results of the two models are still in the same range, above this level the differences in ozone loss are very large. While the maximum in ozone loss for the results of E39/C is located around 450 K, the CLaMS results suggest, that the area of maximum ozone destruction is 50 K higher. Likewise the absolute values of vortex averaged ozone loss derived by E39/C only reach 50% of that derived from a CLaMS simulation carried out with full chemistry.

Another result that can be taken from Figure WP4-22 is a validation of the tracer correlation method with a passively transported ozone tracer. A comparison between the ozone loss derived from the tracer correlation method and the difference between chemically changed ozone and passive ozone shows similar results.

Summarizing it can be said that

- CCMs are by nature comparably coarse-gridded. Due to the fact, that they have to be computationally manageable, they are limited concerning the inclusion of detailed and highly complex parameterisations of physical processes.
- Shortcomings of CCMs can be assessed by the comparison between the CCMs and offline CTMs, driven by the CCMs dynamics, which include a more detailed and complex process parameterisations concerning the chemistry, mixing and microphysical processes, thus quantifying the effects on e. g. ozone loss.

- Reasonal correction and error terms can be derived and applied to the results from CCMs.
    - Example: The minimum arctic ozone column derived by the E39/C for the 2015 timeslice should be corrected for at least 50 DU.
- Suggestions for different parameterisations to be applied in CCMs can be supported by not only qualifying, but quantifying the results to be expected.
- Various scenarios and process studies can be carried out at higher resolution and on a more complex level by CTM runs embedded in CCM experiments like timeslice experiments and long-term transient runs.

Contribution of MPI-MAECHAM

The timeslice experiments with typical conditions for 1960, 1990 and 2000 have been analysed in co-operation with MPI-C. The experiment for 1990 conditions has been evaluated with observations of stratospheric chemical compounds by the HALOE/UARS satellite (Steil et al., 2003). The radiative-chemical-dynamical interaction and the changes from 1960 to 2000 have been analysed in Manzini et al. (2003).

A middle atmosphere climate model with interactive chemistry has been employed for multi-year simulations with fixed boundary conditions for near past and present conditions. Specifically, results from three 20-year equilibrium simulations have been presented: The 1960 simulation for near past condition, characterised by low chlorine and greenhouse gases concentrations, and the 1990 and 2000 simulations with respectively chlorine and greenhouse gases concentration of the early and late 1990. Climatological sea surface temperatures have been specified for each simulation. Most of the results reported here covered the 1960 and 2000 simulations. The main findings of this work are summarised as follow:

1. The atmosphere in the 2000 simulation is globally perturbed with respect to the atmosphere in the 1960 simulation, as shown by the 2000-1960 change in the annual, zonal mean ozone, temperature and water vapour. These average changes are consistent with the observed trends in ozone and temperature as well as previous modelling works.

2. In the Arctic stratosphere, a significant average cooling in March with respect to the 1960 simulation is found only for the 2000 simulation. The difference in the responses of the 1990 and 2000 simulations from our model is indicative of a high sensitivity of the Arctic temperature to the chlorine loading of the atmosphere, because the chemical processes leading to ozone destruction are non-linear. From the analysis of the dynamical response in the stratosphere and mesosphere and given that the tropospheric wave activity is comparable in the simulations, it is concluded that in the 2000 simulation the cooling involves mainly radiative and chemical processes. Therefore, our results support the interpretation that the extreme low temperatures observed in March in the last few decades can arise solely from the radiative-chemical feedback. Although variations in the lower stratospheric temperatures by low frequency modulation of upward propagating wave activity cannot be ruled out, it does not seem to be a necessary factor in our simulations. In the Antarctic, the ozone hole develops in both simulations of the 1990s with respect to the 1960 simulation, and the cooling of the lower stratosphere is substantially larger and longer lasting than in the Arctic.

3. Both planetary and gravity waves play a role in the dynamical response to ozone depletion. Because of the changes in the zonal mean wind caused by ozone depletion (via the temperature changes), the propagation characteristics of the stratosphere in the 1960 and 2000 simulation have been substantially modified. For the planetary waves the change in the propagation characteristics means a positive and local feedback (waves diverted from the polar lower stratosphere). For the gravity waves it means a negative and remote feedback (larger deposition in the mesosphere). The behaviour of the gravity waves is explained by the fact that strong stratospheric westerlies (e.g., the 2000 simulation) imply enhanced filtering of eastward gravity waves and therefore a net gravity wave momentum flux at the stratopause that is more negative than in the case of weak westerlies (e.g., the 1960 simulation). Assuming an isotropic gravity wave spectrum emerging from the lower troposphere, this is a general and plausible result not restricted to the particular gravity wave parameterisation used, although its details and the strength of the response can depend on the parameterisation employed. From March to April, the increase in the downward motion is propagated downward, because of the downward propagation of zonal mean changes due to breaking and dissipation of upward propagating planetary waves.

4. A novel result from our simulations is that a negative dynamical feedback (increased downward motion and associated dynamical heating) is initiated in the mesosphere by the gravity wave

reaction to the increased zonal winds in the stratosphere, during spring in both the Arctic and Antarctic. The difference in the responses in the two hemispheres stems primarily from the different average states, a consequence of the more active planetary waves in the northern hemisphere. While also in our model the positive feedback of the planetary waves may exacerbate ozone depletion (as proposed by Austin et al. (1992) and Shindell et al. (1998), among others), it is plausible that the negative feedback of the gravity waves can limit the cooling and the strengthening of the lower stratospheric polar vortex from above, therefore facilitating ozone recovery.

5. In both hemispheres the area covered with PSCs increases significantly in spring, contributing to the chemical-radiative-dynamical feedbacks. Chlorine partitioning in polar springs changes strongly from the 1960 to 2000, while for the amount of total reactive nitrogen the increase from the N_2O increase is approximately compensated by enhanced de-nitrification.

Although in the current work it does not appear to be a dominant effect, the comparison of the 1960 and 2000 simulations suggests that ozone depletion might perturb also the wave propagation into the stratosphere, or at the least the frequency of occurrence of months with low heat fluxes. In a future work, it would be of interest to investigate the relevance of these possible changes for the troposphere.

The reported changes in the mesosphere motivate the development of models with tops in the upper atmosphere, for use in climate change assessments. Currently this type of model still has a crude representation of mesospheric processes. In the MAECHAM4/CHEM model, the upper mesosphere is essentially a buffer zone. Nevertheless, the effects of gravity wave breaking have been here taken into account in a comprehensive way, by using a parameterisation that considers a spectrum of gravity waves. However, the forcing of the gravity waves was not changed between the simulations, while it might if the meteorological variability of the troposphere does change. In a natural extension of this work, it would therefore be of interest to specify the forcing of the gravity waves from the simulated meteorological disturbances.

Joint contribution from MPI-C and MPI-MAECHAM

The importance of feedback between chemistry and dynamics

In order to assess the role of interactive chemistry (e.g. prognostic ozone) on the variability of the stratosphere, in Steil et al. (2003) an additional simulation has been performed with the MAECHAM4 model without the CHEM chemistry module and instead a prescribed climatological ozone distribution. The prescribed ozone climatology is the monthly zonal mean ozone presented in Fortuin and Kelder (1998). Figure WP4-23 (upper panel) depicts the daily and inter-annual variability associated with sudden stratospheric warming at 30 hPa (compare with Fig. WP4-6).

Clearly the level of dynamical activity is comparable in the two models at the North Pole, because of the dominant role played by planetary waves in determining the temperature in the polar winter and spring stratosphere. A similar behaviour is found also lower down at 70 hPa. Consistent with these findings, there is no statistically significant difference in the average temperatures in the North polar lower stratosphere (see the upper panel of figure WP4-8).

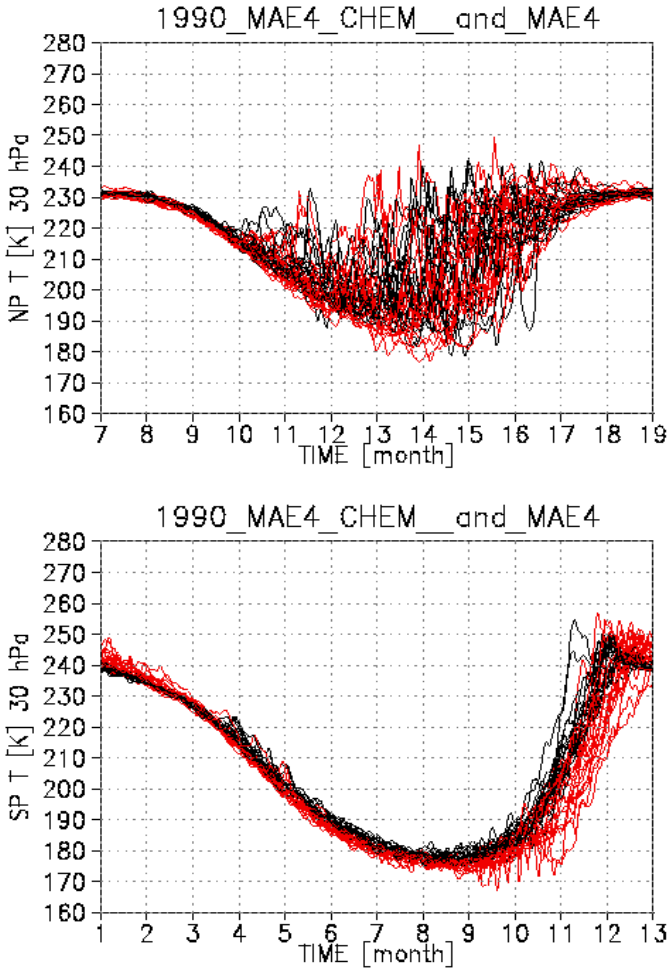

Figure WP4-23: Daily North (upper) and South (lower) Pole temperature at 30hPa. Black: from the 20 years simulation with the model without chemistry. Red: from the 20 year simulation with the model that includes interactive chemistry**.**

At the South Pole instead (Figure WP4-24 lower panel), there is a statistically significant shift to lower temperature (from 5 to 10 K in October and between 10 and 14 K in November) in the average temperature. Concerning daily and inter-annual variability, Figure WP4-23 (lower panel) shows that both models are characterised by much less variability in the Southern polar region (with respect to the

Northern polar region). For both models the variability is confined to the spring season, a realistic behaviour although variability at the beginning of the spring could be underestimated because of the model cold bias in the upper stratosphere. The comparison between the two models suggests an enhancement of the inter-annual (but not daily) variability in October, November and December in the model with interactive chemistry (e.g., wider temperature excursions for the red curves with respect to the black curves). Presumably, the temperature inter-annual variability is larger in the interactive model because low ozone in dynamically quiet years feeds back to produce additional cooling.

In summary, for the climate and chemical composition typical of 1990, the positive radiative-dynamical feedback between ozone depletion and temperature does play a role in determining the average temperature and the polar inter-annual variability in the southern hemisphere during spring, while the northern hemisphere is dominated by the dynamical forcing, except at very low heat fluxes.

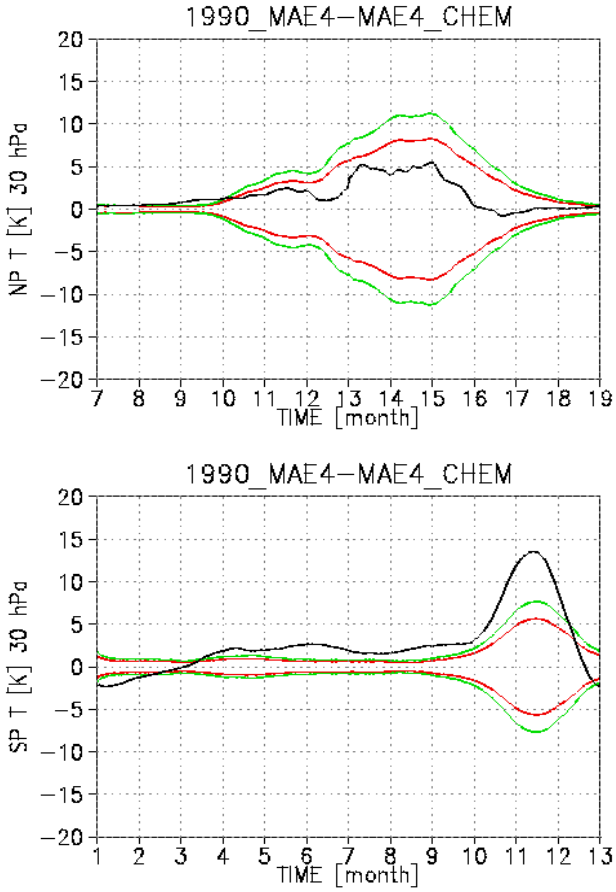

Figure WP4-24: 20 year ensemble average of the 31-day running mean temperature differences (without - with interactive chemistry) at 30 hPa at the poles. The red (green) curve is the envelope outside which the difference is significant at the 95% (99%).

Ozone and temperature changes in Arctic spring

As described in Manzini et al. (2002), in the Arctic lower stratosphere, a cooling in March with respect to the 1960 simulation is found only for the 2000 simulation but not for the 1990 simulation. Wave activity emerging from the troposphere is found to be comparable in the winters of the 1960 and 2000 simulations, suggesting that ozone depletion and greenhouse gases increase contribute to the 2000-1960 March cooling in the Arctic lower stratosphere. These results therefore provide support to the interpretation that the extreme low temperatures observed in March in the last decade can arise from radiative and chemical processes, although other factor cannot be ruled out. The comparison of the 1960 and 2000 simulations shows an increase in down welling in the mesosphere at the time of cooling in the lower stratosphere (in March in the Arctic; in October in the Antarctic). The

mesospheric increase in down welling can be explained as the response of the gravity waves to the stronger winds associated with the cooling in the lower stratosphere. Planetary waves appear to contribute to the downward shift of the increased down welling, with delay of about a month. The increase in dynamical heating associated with the increased down welling may limit the cooling and the strengthening of the lower stratospheric polar vortex from above, facilitating ozone recovery and providing a negative dynamical feedback. In both the Arctic and Antarctic, the cooling from ozone depletion is found to affect the area covered with polar stratospheric clouds in spring, which is substantially increased from the 1960 to the 2000 simulations. In turn, increased amounts of PSCs can facilitate further ozone depletion in the 2000 simulation.

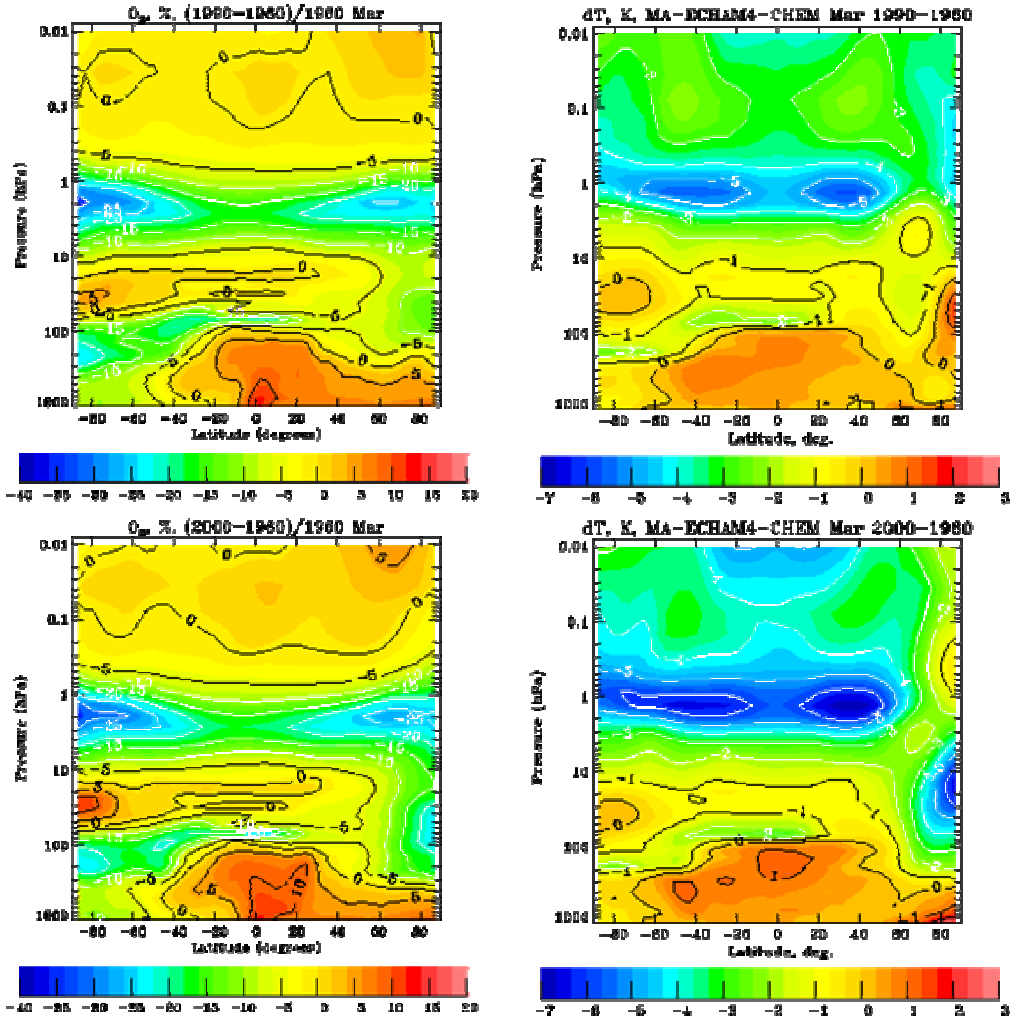

Figure WP4-25: Ozone and temperature changes for the 1990 and 2000 timeslices against the 1960 timeslice as calculated by MAECHAM4/CHEM. 20 year averages for March.

In the lower stratosphere the 2000-1960 change for the months of March and April is characterised by a pronounced cooling (–4 to –5 K), statistically significant at the 95% level. The temperature difference is no longer significant in the upper stratosphere in March, where the inter-annual variability in the model is larger. On average, in April a slight warming (1 K) appears in the upper stratosphere. Another view of the difference in the temperature and ozone changes, 1990-1960 and 2000-1960 respectively, is given in Figure WP4-25, where their respective changes in March zonal mean temperature and percentage ozone are shown. Concerning ozone, the relative change is similar for 1990-1960 and 2000-1960 in the mesosphere, upper stratosphere and southern polar stratosphere. In the northern polar stratosphere instead, the 2000-1960 relative change reaches –20%, about twice that for the 1990-1960 change. Concerning the temperature, the middle atmosphere in general is about one degree colder in 2000 than in 1990. The major difference between the 1990-1960 and 2000-1960

changes is again found in the Arctic middle atmosphere: while the lower stratosphere is warmer in the 1990 simulation with respect to the 1960 simulation, it is up to 6 K colder in the 2000 simulation with respect to the 1960 simulation. Above, in the mesosphere, respective opposite changes are found, as a results of changed dynamics.

Joint contribution of MPI-MAECHAM, MPI-C, DLR

In 2002, all available fully coupled chemistry-climate models (CCMs) including MAECHAM4/CHEM and E39/C have simulated the impacts of recent and future GHG and halogen changes on ozone depletion and recovery (Austin et al., 2003). The results of this international model inter-comparison project have been considered in the UNEP/WMO "Scientific Assessment of Ozone Depletion: 2002" (2003) and the EU-report on ozone-climate interactions (2003).

The employed CCMs cover a wide range of timescales of integration and vary considerably in complexity. The results of specific diagnostics have been analysed to examine the agreements and differences amongst individual models and observations. The examination of model results with respective observations, particularly long-term and global observations as provided by ground-based stations and satellites, is the basis for the detection and evaluation of model deficiencies which is important for the assessment of the consistency of model predictions. Since individual model simulations with coupled chemistry-climate models are time consuming and expensive and due to limited computer power, each model system can only be run for a very few number of model simulations. Therefore, one way to estimate the current abilities of CCMs is to compare the results of already existing simulations which assume similar boundary conditions. Following this philosophy, Austin and co-workers identified a number of shortcomings in the employed models.

Many models indicate a significant cold bias at high latitudes, particular in the Southern Hemisphere during winter and spring. Another unsolved problem is that none of these models is able to reproduce the observed water vapour trend in the (lower) stratosphere. As a result of the widely differing modelled polar temperatures and water vapour mixing ratios, different amounts of polar stratospheric clouds are simulated which in turn result in varying ozone values in the models (Figure WP4-26). Additionally, it must be noted that none of the currently available (chemistry-) climate models have been ever simulated a major stratospheric warming event in the Southern Hemisphere, which was observed in September 2002. This indicates to further deficiencies in the models which might be related to an inadequate representation of planetary wave activity, i.e., the forcing mechanisms in the troposphere and the upward propagation into the stratosphere. Nevertheless, the available CCMs have been employed to determine the possible future behaviour of ozone. The differences in the model predictions can also be used as an assessment for the degree of uncertainty of such estimates. All models predict eventual ozone recovery, but they give a range of results concerning its timing and extent. In the Antarctic, the models mostly agree suggesting that stratospheric ozone columns in spring time (ozone hole) have probably reached almost the lowest values although the vertical and horizontal extent of depletion may increase slightly further over the next few years. For the Arctic it is much more difficult to determine the start of ozone recovery since inter-annual variability due to dynamic processes will tend to mask the signal. On the other hand it is still an open question whether climate change will lead to a decrease in stratospheric temperature in northern winter (due to radiative cooling caused by enhanced GHG concentrations) or if this effect is reduced or overcompensated by dynamic heating (due to enhanced activity of planetary wave generated in a warmer troposphere). This open question is a central point for further investigations of the recovery of the ozone layer. It points towards the importance of the feedback of climate change and atmospheric chemistry.

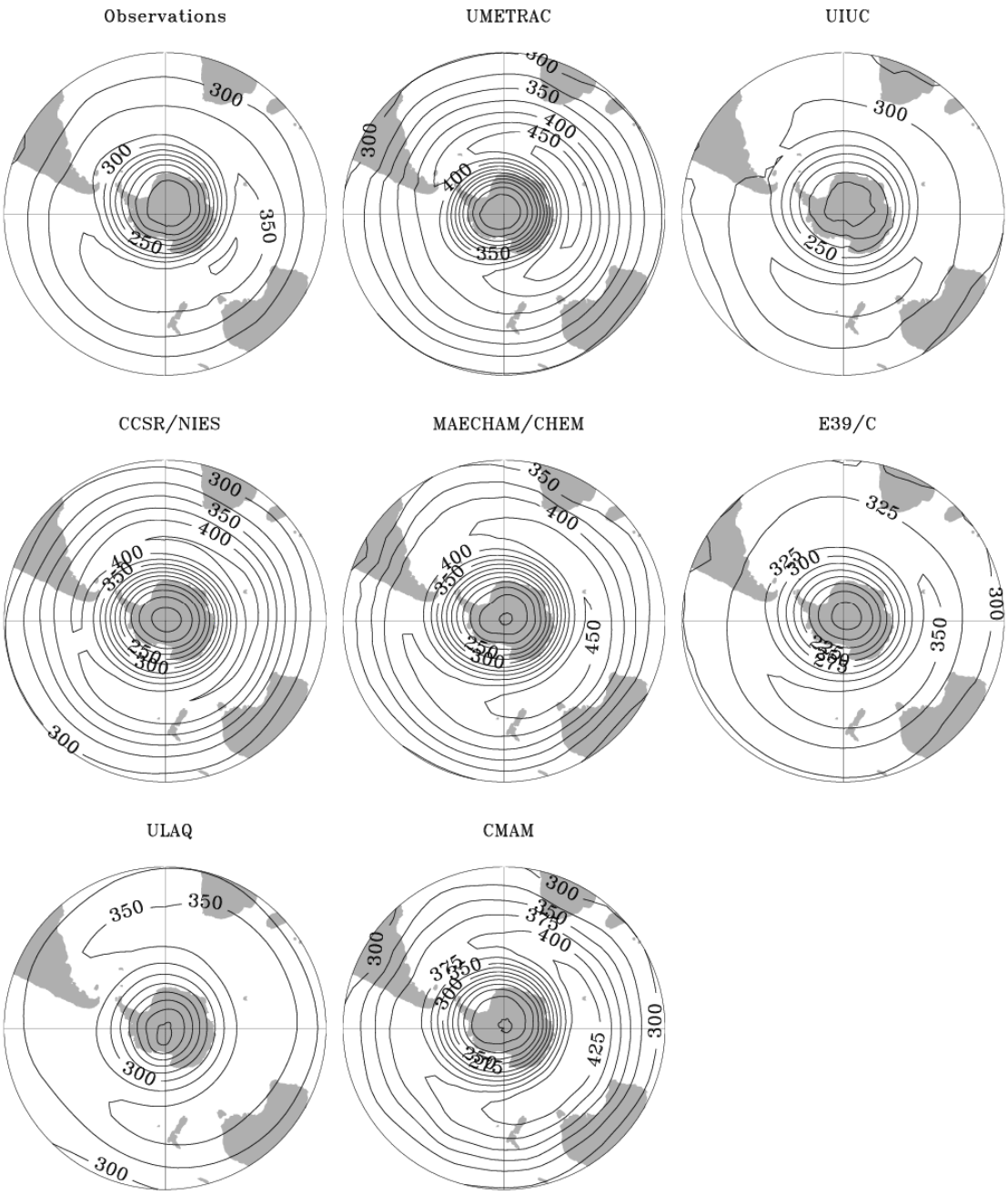

Figure WP4-26: Monthly mean values of southern hemisphere total ozone columns of October as simulated by different CCMs (UMETRAC: mean 1980-2000; CMAM: 2000; MAECHAM4/CHEM: 2000; E39/C: 1990; CCSR/NIES: mean 1990-1999; UIUC: 1995; ULAQ: 1990). Observations are from satellite measurements for the period 1993-2000 (adopted from Austin et al., 2003).

New publications with contributions from WP 4

Austin, J., D. Shindell, S.R. Beagley, C. Brühl, M. Dameris, E. Manzini, T. Nagashima, P. Newman, S. Pawson, G. Pitari, E. Rozanov, C. Schnadt, and T.G. Shepherd, Uncertainties and assessments of chemistry-climate models of the stratosphere, Atmos. Chem. Phys., 3, 1-27, 2003.

Konopka, P., J.-U. Grooss, G. Günther, D. S. McKenna, R. Müller, J. W. Elkins, D. Fahey, and P. Popp, Weak impact of mixing on chlorine deactivation during SOLVE/THESEO2000: Lagrangian modelling (CLaMS) versus ER-2 in situ observations, J. Geophys. Res., 108, 8324, doi:10.1029/2001JD000876, 2003.

Lamago, D., M. Dameris, C. Schnadt, V. Eyring, and C. Brühl, Impact of large solar zenith angles on lower stratospheric dynamical and chemical processes in a coupled chemistry-climate model, Atmos. Chem. Phys., 3, 1981-1990, 2003.

Manzini, E., B. Steil, C. Brühl, M. A. Giorgetta, and K. Krüger, A new interactive chemistry-climate model: 2. Sensitivity of the middle atmosphere to ozone depletion and increase in greenhouse gases and implications for recent stratospheric cooling, J. Geophys. Res., 108(D14), 4429, doi:10.1029/2002JD002977, 2003.

Schnadt, C., M. Dameris, M. Ponater, R. Hein, V. Grewe, and B. Steil, Interaction of atmospheric chemistry and climate and its impact on stratospheric ozone, Climate Dynamics, 18, 501-517, 2002.

Schnadt, C. and M. Dameris, Relationship between North Atlantic Oscillation changes and an accelerated recovery of stratospheric ozone in the northern hemisphere, Geophys. Res. Lett., 30, 1487, doi:10.1029/2003GL017006, 2003.

Steil, B., C. Brühl, E. Manzini, P.J. Crutzen, J. Lelieveld, P.J Rasch, E. Roeckner, K. Krüger, A new interactive chemistry climate model. I: Present day climatology and interannual variability of the middle atmosphere using the model and 9 years of HALOE/UARS data. J. Geophys. Res., 108(D9), 4290, doi:10.1029/2002JD002971, 2003.

Steinbrecht, W., Claude, H., Köhler, U., and Hoinka, K. P., Correlations between tropopause height and total ozone: implications for long-term changes, J. Geophys. Res., 103 , 19183-19192, 1998.

Steinbrecht, W., Claude, H., Köhler, U., and Winkler, P., Interannual changes of total ozone and northern hemisphere circulation patterns, Geophys. Res. Lett., 28, 1191-1194, 2001.

Tilmes, S., R. Müller, J.-U. Grooss, and J.M. Russell, Ozone loss and chlorine activation in the Arctic winters 1991-2003 derived with the TRAC method, Atmos. Chem. Phys. Diss., accepted, 2004.

Timmreck, C., Three-dimensional simulation of stratospheric background aerosol: First results of a multi-annual GCM simulation, J. Geophys. Res., 106, 28313-28332, 2001.

Vehkamäki, H., M. Kulmala, I. Napari, K. E. J. Lehtinen, C. Timmreck, M. Noppel and A. Laaksonen, An improved parameterization for sulfuric acid/water nucleation rates for tropospheric and stratospheric conditions J. Geophys. Res. 107, 4622, doi:10.1029/2002JD002184, 2002.

Diploma Thesis

Götzfried, K., Modellierte Partitionierung von NO_y in der Stratosphäre im Vergleich mit Messdaten, Ludwig-Maximilians Universität München, pp. 85, 2003.

Lamago, D., Quantifizierung chemischer und dynamischer Effekte großer Zenitwinkel in einem globalen Klima-Chemie-Modell, Technische Universität München, pp. 110, 2002.

References

Austin, J., N. Butchart, and K.P. Shine, Possibility of an Arctic ozone hole due to doubled-CO2 climate, Nature, 360, 221-225, 1992.

Benkovitz, C.M., Scholtz, M. T., Pacyna, J., Tarrason, L., Dignon, J., Voldner, E. C., Spiro, P. A., Logan, J. A., and Graedel, T. E., Global gridded inventories of anthropogenic emissions of sulfur and nitrogen, J. Geophys. Res., 101, 29239-29253, 1996.

Bojkov, R.D. and Fioletov, V. E., Estimating the global ozone characteristics during the last 30 years, J. Geophys. Res., 100, 16537-16551, 1995.
Brühl, C. and Crutzen, P. J., MPIC two-dimensional model, NASA Ref. Publ. 1292, 103-104, 1993.
Chubachi, S., A special ozone observation at Syowa Station, Antarctica from February 1982 to January 1983, Atmospheric Ozone: Proceedings of the Quadrennial Ozone Symposium, C.S. Zerefos and A.M. Ghazi (Eds.), Halkidiki, Greece, 3-7 September 1984, 285-289, 1985.
Farman, J. C., Gardiner, B. G., and Shanklin, J. D., Large losses of total ozone in Antarctica reveal seasonal ClOx/NOx interaction, Nature, 315, 207-210, 1985.
Fortuin, J. P. F. and Kelder, H., An ozone climatology based on ozonesonde and satellite measurements, J. Geophys. Res., 103, 31709-31734, 1998.
Hao, W. M., Liu, M.-H. and Crutzen, P. J., Estimates of annual and regional releases of CO2 and other trace gases to the atmosphere from fires in the tropics, based on the FAO statistics for the period 1975-1980, In: Fire in the Tropical Biota, Ecological Studies 84, J.G. Goldammer (Ed.), Springer-Verlag, New York, USA, 440-462, 1990.
Hein, R., Dameris, M., Schnadt, C., Land, C., Grewe, V., Köhler, I., Ponater, M., Sausen, R., Steil, B., Landgraf, J., Brühl, C., Results of an interactively coupled atmospheric chemistry-general circulation model: Comparison with observations, Ann. Geophysicae, 19 , 435-457, 2001.
Hermann et al, Meridional distributions of aerosol particle number concentrations in the upper tropopsphere and lower stratosphere obtaind by Civil Aircraft for Regular Investigation of the Atmosphere Baes on an Intrument Container(CARIBIC) flights, J. Geophys. Res. 108, D3, 4114, doi:10.1029/2001JD00107, 2003.
IPCC (Intergovernmental Panel on Climate Change), Special report on aviation and the global atmosphere, J.E. Penner, D.H. Lister, D.J. Griggs, D.J. Dokken, M. McFarland (Eds.), Cambridge University Press, Cambridge, United Kingdom and New York, NY, USA, 373pp., 1999.
IPCC (Intergovernmental Panel on Climate Change), Climate change 2001: The scientific basis. Contribution of Working Group 1 to the Third Assessment Report, J.T.~Houghton (Eds.), Cambridge University Press, Cambridge, United Kingdom and New York, NY, USA, 881pp., 2001.
Kirchner, I., Stenchikov, G. L., Graf, H.-F., Robock, A., and Antuna, J. C., Climate model simulation of winter warming and summer cooling following the 1991 Mount Pinatubo volcanic eruption, J. Geophys. Res., 104, 19039-19055, 1999.
Köhler, H. W., Estimation of NOx and other emissions from merchant ocean-going ships, Shipping World and Shipbuilder, Sutton, Surrey, UK, Vol. 204, 33--36, 2003.
Krämer, M., Ri. Müller, H. Bovensmann, J. Burrows, J. Brinkmann, E.P. Röth, J.-U. Grooss, Ro. Müller, T. Woyke, R. Ruhnke, G. Günther, J. Hendricks, E. Lippert, K.S. Carslaw, T. Peter, A. Zieger, C. Brühl, B. Steil, R. Lehmann, and D.S. McKenna, Intercomparison of stratospheric chemistry models under polar vortex conditions, J. Atmos. Chem., 45, 51-77, 2003.
Land, C., Feichter, J., and Sausen, R., Impact of vertical resolution on the transport of passive tracers in the ECHAM4 model, Tellus, 54B, 344-360, 2002.
Landgraf, J. and Crutzen, P. J., An efficient method for online calculations of photolysis and heating rates, J. Atmos. Sci., 55, 863-878, 1998.
Matthes, S., Globale Auswirkungen des Straßenverkehrs auf die chemische Zusammensetzung der Atmosphäre, PhD thesis, Ludwig-Maximilians Universität München, DLR-Report 2003-15, ISSN 1434-8454, 160pp., 2003.
McPeters, R. D., Hollandsworth, S. M., Flynn, L. E., Herman, J. R., and Seftor, C. J., Long-term ozone trends derived from the 16-year combined Nimbus 7/Meteor 3 TOMS version 7 record, Geophys. Res. Lett., 23, 3699-3702, 1996.
Moldanova, J., R. Bergström, and J. Langner, A photolysis scheme for photochemical modelling of the troposphere and lower stratosphere, A contribution to the EUROTRAC-2 subproject GLOREAM, Proceedings from the EUROTRAC-2 Symposium, Garmisch-Partenkirchen, 2002.
Randel et al., Ozone and temperature changes in the stratosphere following the eruption of Mount Pinatubo, J. Geophys. Res., 100, 16,753-16,764, 1995.
Randel, W. J., Wu, F., Oltmans, S. J., Rosenlof, K., and Nedoluha, G. E., Interannual changes of stratospheric water vapor and correlations with tropical tropopause temperatures, J. Atmos. Sci., in press, 2004.

Schmitt, A., and Brunner, B., Emissions from aviation and their development over time, in Pollutants from air traffic - results of atmospheric research 1992-1997, DLR-Mitt. 97-04, U. Schumann et al. (Eds.), 37-52, DLR Köln, Germany, 1997.

Shindell, D.T., D. Rind, and P. Lonergan, Increased polar stratospheric ozone losses and delayed eventual recovery owing to increased greenhouse-gas concentrations, Nature, 392, 589-592, 1998.

Steil, B., Dameris, M., Br\"uhl, C., Crutzen, P. J., Grewe, V., Ponater, M., and Sausen, R., Development of a chemistry module for GCMs: first results of a multiannual integration, Ann. Geophysicae, 16, 205-228, 1998.

WMO (World Meteorological Organisation), Scientific Assessment of Ozone depletion: 2002, Global Ozone Research and Monitoring Project, Report No. 47, ISBN 92-807-2261-1, 498pp., 2003.